Ocean Modelling 34 (2010) 70–91

Contents lists available at ScienceDirect

Ocean Modelling

journal homepage: www.elsevier.com/locate/ocemod

Ocean turbulence, III: New GISS vertical mixing scheme

V.M. Canuto [a,b,*], A.M. Howard [a,c], Y. Cheng [a,d], C.J. Muller [e], A. Leboissetier [a,e], S.R. Jayne [f]

[a] NASA, Goddard Institute for Space Studies, New York, NY, 10025, USA
[b] Department of Applied Physics and Applied Mathematics, Columbia University, New York, NY, 10027, USA
[c] Department of Physical Environmental and Computer Science, Medgar Evers College, CUNY, New York, NY, 11225, USA
[d] Center for Climate Systems Research, Columbia University, New York, NY, 10025, USA
[e] Department of Earth, Atmospheric and Planetary Sciences, MIT, Cambridge, MA, 02138, USA
[f] Physical Oceanography Department, WHOI, Woods Hole, MA, 02543, USA

ARTICLE INFO

Article history:
Received 5 June 2008
Received in revised form 20 April 2010
Accepted 27 April 2010
Available online 12 May 2010

The authors dedicate this work to the memory of Peter Killworth.

Keywords:
Turbulence
Tides
Double diffusion
Mixing
OGCM

ABSTRACT

We have found a new way to express the solutions of the RSM (Reynolds Stress Model) equations that allows us to present the turbulent diffusivities for heat, salt and momentum in a way that is considerably simpler and thus easier to implement than in previous work. The RSM provides the dimensionless *mixing efficiencies* Γ_α (α stands for heat, salt and momentum). However, to compute the diffusivities, one needs additional information, specifically, the dissipation ε. Since a dynamic equation for the latter that includes the physical processes relevant to the ocean is still not available, one must resort to different sources of information outside the RSM to obtain a complete *Mixing Scheme* usable in OGCMs.

As for the RSM results, we show that the Γ_α's are functions of both *Ri* and R_ρ (Richardson number and density ratio representing double diffusion, DD); the Γ_α are different for heat, salt and momentum; in the case of heat, the traditional value $\Gamma_h = 0.2$ is valid only in the presence of strong shear (when DD is inoperative) while when shear subsides, NATRE data show that Γ_h can be three times as large, a result that we reproduce. The salt Γ_s is given in terms of Γ_h. The momentum Γ_m has thus far been guessed with different prescriptions while the RSM provides a well defined expression for $\Gamma_m(Ri, R_\rho)$. Having tested Γ_h, we then test the momentum Γ_m by showing that the turbulent Prandtl number Γ_m/Γ_h vs. *Ri* reproduces the available data quite well.

As for the dissipation ε, we use different representations, one for the mixed layer (ML), one for the thermocline and one for the ocean's bottom. For the ML, we adopt a procedure analogous to the one successfully used in PB (planetary boundary layer) studies; for the thermocline, we employ an expression for the variable εN^{-2} from studies of the internal gravity waves spectra which includes a latitude dependence; for the ocean bottom, we adopt the enhanced bottom diffusivity expression used by previous authors but with a state of the art internal tidal energy formulation and replace the fixed $\Gamma_\alpha = 0.2$ with the RSM result that brings into the problem the *Ri*, R_ρ dependence of the Γ_α; the unresolved bottom drag, which has thus far been either ignored or modeled with heuristic relations, is modeled using a formalism we previously developed and tested in PBL studies.

We carried out several tests without an OGCM. Prandtl and flux Richardson numbers vs. *Ri*. The RSM model reproduces both types of data satisfactorily. DD and Mixing efficiency $\Gamma_h(Ri, R_\rho)$. The RSM model reproduces well the NATRE data. Bimodal ε-distribution. NATRE data show that $\varepsilon(Ri < 1) \approx 10\varepsilon(Ri > 1)$, which our model reproduces. Heat to salt flux ratio. In the $Ri \gg 1$ regime, the RSM predictions reproduce the data satisfactorily. NATRE mass diffusivity. The z-profile of the mass diffusivity reproduces well the measurements at NATRE. The local form of the mixing scheme is algebraic with one cubic equation to solve.

Published by Elsevier Ltd.

1. Introduction

In two previous studies (Canuto et al., 2001, 2002, cited as I and II), two vertical mixing schemes for coarse resolution OGCMs (ocean general circulation models) were derived and tested. However, because of shortcomings in I, II of both physical and structural nature, a new mixing scheme became necessary which we present

* Corresponding author at: NASA, Goddard Institute for Space Studies, New York, NY, 10025, USA. Tel.: +1 212 6785571; fax: +1 212 6785560.
E-mail addresses: vcanuto@giss.nasa.gov, vmcanuto@gmail.com (V.M. Canuto).

1463-5003/$ - see front matter Published by Elsevier Ltd.
doi:10.1016/j.ocemod.2010.04.006

here. By structural we mean that the expressions for the heat, salt and momentum diffusivities in I, II were rather cumbersome. By physical, we mean the need to include important physical processes that were missing in I, II.

Concerning the structural issue, we have found a new solution of the *Reynolds Stress Model*, RSM, that yields expressions for the diffusivities that are simpler and thus easier to code than the ones in II. If we denoted by K_α the diffusivities for momentum, heat and salt (subscript α), the new solutions of the RSM are:

$$\text{Mixed layer}: \quad K_\alpha = S_\alpha \frac{2K^2}{\varepsilon}, \tag{1a}$$

$$\text{Deep Ocean}: \quad K_\alpha = \Gamma_\alpha \frac{\varepsilon}{N^2}, \quad \Gamma_\alpha \equiv \frac{1}{2}(\tau N)^2 S_\alpha \tag{1b}$$

Here, K is the eddy kinetic energy, ε its rate of dissipation, N is the Brunt–Vaisala frequency with $N^2 = -g\rho^{-1}\rho_z$, $\tau = 2K\varepsilon^{-1}$ is the dynamical time scale and S_α are dimensionless *structure functions* which are functions of:

$$S_\alpha(Ri, R_\rho, \tau N) \tag{2a}$$

where the Richardson number Ri and the density ratio R_ρ (characterizing double diffusion DD processes) are defined as follows:

$$Ri = \frac{N^2}{\Sigma^2}, \quad R_\rho = \frac{\alpha_S \partial S/\partial z}{\alpha_T \partial T/\partial z} \tag{2b}$$

Here, the variables T, S and $\mathbf{U}$ represent the mean potential temperature, salinity and velocity. The thermal expansion and haline contraction coefficients $\alpha_{T,S} = (-\rho^{-1}\partial\rho/\partial T, +\rho^{-1}\partial\rho/\partial S)$ may be computed using the non-linear UNESCO equation of state and $\Sigma = (2S_{ij}S_{ij})^{1/2}$ is the mean shear with $2S_{ij} = U_{i,j} + U_{j,i}$, where the indices $i, j = 1, 2, 3$ and $a_{,i} \equiv \partial a/\partial x_i$. Relations (1a) and (1b) contain two unknown variables, the dissipation ε and the eddy kinetic energy K:

$$\varepsilon, \qquad \tau = \frac{2K}{\varepsilon} \tag{3}$$

which means that to complete the RSM, one must add two more relations that provide the variables (3). In engineering flows, these two variables are traditionally obtained by solving the so-called K–ε model which means two differential equations for those two variables. The solution of the K–ε model, represented by Eq. (20), would close the problem since every variable would now be expressed in terms of the large scale fields. Let us analyze how these two variables are determined in the present oceanic context.

1.1. Determination of τ

Since most of the ocean is stably stratified, the vertical extent of the eddies is much smaller than the vertical scale of density variation (except of course in deep convection places), a local approach to the kinetic energy equation, first relation in Eq. (20), is a sensible one. Physically, this is equivalent to taking production equal dissipation, $P = \varepsilon$, where $P = P_s + P_b$ is the total production due to shear and buoyancy. Since $P = K_m\Sigma^2 - K_\rho N^2$, the derivation is presented in Eqs. (22), (23), (54) and (55), use of relations (1b) in $P = \varepsilon$ transforms the latter into an algebraic equation for the variable τ given by Eqs. (40) and (41) the result of which is the function:

$$\tau = \tau(Ri, R_\rho) \tag{4}$$

Use of (4) in the second of (1b) and in (2a) yields the structure functions and the *mixing efficiencies* in terms of the large scale variables:

$$S_\alpha(Ri, R_\rho), \quad \Gamma_\alpha(Ri, R_\rho) \tag{5}$$

Let us note that the above procedure applies in principle to the mixed layer, the thermocline and the ocean bottom. The problem is to know how to determine the Richardson number in each region, a problem we discuss in Sections 6 and 7.3. When applied to the mixed layer, the above determination of the mixing efficiencies is physically equivalent to assuming that the external wind directly generates oceanic mixing. There is, however, a second possibility, namely that the wind first generates surface waves which then become unstable and break, generating mixing (Craig and Banner, 1994; Umlauf and Burchard, 2005). To account for such a process, one needs the full K-equation in (20) with a non-zero flux F_K of K for which one needs a closure. The K-flux F_K is a third-order moment and, as discussed in Cheng et al. (2005), there is still a great deal of uncertainty on how to close such higher-order moments. The wave breaking phenomenon is introduced into the problem by taking the value of F_K at the surface $z = 0$ equal to the power provided by the wave breaking model, as described in the two references just cited. In the present case, local limit $P = \varepsilon$, relations (5) are still not sufficient to determine the diffusivities given by the first relation in (1b) for we require the dissipation ε whose determination we discuss next.

1.2. Determination of ε

In principle, one could solve the second of Eq. (20) and obtain the dissipation $\varepsilon(Ri, R_\rho)$ in analogy with the procedure that lead to relations (5). Regrettably, such a procedure is not feasible since the equation for ε has been problematic since the RSM was first employed by Mellor and Yamada (1982). The reason is that, contrary to the K-equation whose exact form can be derived from turbulence models, the ε-equation has thus far been entirely empirically based and a form that includes stable stratification, unstable stratification and double diffusion, does not exist in the literature. Recently, some progress has been made in deriving an ε-equation from first principles (Canuto et al., 2010) but only for the case of unstable stratification, while most of the ocean is stably stratified. For these reasons, we still cannot employ the dynamic equation for ε and we must rely on a different approach. As for the *mixed layer*, we shall employ the length scheme discussed in Section 6, leading us to relations (62)–(64).[1] In the *thermocline*, we borrow from the IGW (internal gravity waves) studies-parameterizations by several authors (Polzin et al., 1995; Polzin, 1996; Kunze and Sanford, 1996; Gregg et al., 1996; Toole, 1998) the form of ε, more precisely, of εN^{-2}, that contains the dependence on latitude given by Eqs. (65)–(68) which should lead to a sharper tropical thermocline. As for the *ocean bottom*, first we include the enhanced bottom diffusivity due to tides, Eq. (70) as suggested by previous authors but with the latest representation of the function $E(x, y)$ (Jayne, 2009), as well as relation (5) instead of the value $\Gamma = 0.2$ used in all previous studies (St. Laurent et al., 2002; Simmons et al., 2004; Saenko and Merryfield, 2005); second, the tidal drag given by Eq. (72) contains a tidal velocity which thus far has been taken to be a constant while we suggest it should be computed consistently with the same tidal model that provides the function $E(x, y)$, as we explicitly discuss in the lines after Eq. (72); third, the component of the tidal field not aligned with the mean velocity cannot be modeled as a tidal drag. Since its mean shear is large, it gives rise to a *large unresolved shear*with respect to the ocean's bottom. This process, which lowers the local Ri below $Ri = O(1)$ allowing shear instabilities to enhance the diffusivities, was recognized only in one work by Lee et al. (2006) who employed an empirical expression for it. Rather, we adopt the knowledge we acquired in dealing with the same problem in the PBL (Cheng et al., 2002) which gives rise to relation (73) which was tested and assessed in previous work and which was shown to work pretty well.

[1] The 1D-GOTM ocean model (Burchard, 2002) has included and solved the ε-equation in the mixed layer.

1.3. Determination of Ri(cr)

It is part of any RSM to determine whether there is a critical Ri(cr) above which mixing vanishes, as it was assumed in the literature for many years. The Mellor and Yamada (1982) model predicted $Ri(\mathrm{cr}) = 0.19$ which was shown to be so low that the resulting mixed layer depths were far too shallow to be acceptable (Martin, 1985). In our opinion, the MY result was a motivation for the KPP model (which is not based on a turbulence closure) since its authors believed that turbulence based models could not give better results. Model I yielded an Ri(cr) not 0.19 but $O(1)$ and more recently (Canuto et al., 2008a) we showed that there is no Ri(cr) at all, as several data of very different nature have now established beyond any reasonable doubt. In particular, the new data have shown that while the heat flux still decreases toward zero at $Ri > 1$, the momentum flux does not, which means that the surface wind stresses are transported deeper than in models with $Ri(\mathrm{cr}) = O(1)$. Before using the new mixing scheme in a coarse resolution OGCM, and in the spirit of previous schemes such as KPP (Large et al., 1994), we carried out a series of tests without an OGCM which we briefly describe below.

(1) In the presence of strong shear, the model predicts that heat and salt diffusivities become identical, as expected.
(2) The model predicts that salt fingers become prevalent at a critical density ratio $R_\rho \approx 0.6$, in agreement with measurements.
(3) Momentum diffusivity $K_m(Ri, R_\rho)$; most mixing schemes (e.g., the KPP model, Large et al., 1994) employ heuristic arguments. Though lack of direct data does not allow a direct assessment of the model prediction of this variable, the predicted Prandtl number σ_t (= ratio of momentum to heat diffusivities) is shown to reproduce well the measured data vs. Ri for the no-DD case, Fig. 3c. Most OGCMs assume $\sigma_t = 10$ which corresponds to $Ri = O(1)$.
(4) On the basis of temperature microstructure measurements, it was generally assumed that $\Gamma_h = 0.2$. Using data from NATRE, St. Laurent and Schmitt (1999), cited as SS99, have, however, shown that such a value is valid only in regions of strong shear and no double diffusion. In the opposite regime of weak shear and strong DD, Γ_h can be 3–4 times larger. The RSM results yield a $\Gamma_h(Ri, R_\rho)$ that fits the data, Fig. 4, quite well.
(5) NATRE data have revealed a bimodal distribution of the energy dissipation rate ε: in the high ε, shear dominated $Ri < 1$ regime, the dissipation is an order of magnitude larger than in the low ε, salt finger dominated $Ri > 1$ regime, a feature that we reproduce reasonably well, Fig. 5a.
(6) The heat to salt flux ratio $r(Ri, R_\rho)$ for $Ri > 1$ reproduces well the values measured at NATRE, as well as laboratory measurements, Fig. 5b.
(7) The profile of the mass diffusivity K_ρ at NATRE reproduces well the measurements, Fig. 9.
(8) In the thermocline, in locations where there is no Double Diffusion, the RSM model predicts that for $Ri(bg) = 0.5$ we have $\Gamma_h = \Gamma_s = 0.2$, $\Gamma_m = 0.6$; while the first two relations are as expected, the momentum mixing efficiency turns out to be three times as large as those of heat and salt.

In summary, the complete *Mixing Scheme* is a combination of results from the RSM which lead to a new determination of the mixing efficiencies (5) plus prescriptions of how to compute the dissipation ε, the latter being different in different parts of the ocean. It is only by combining these two parts that one obtains a complete mixing scheme that can be used in an OGCM.

2. Overview of previous and present mixing models

Ocean general circulation models (OGCMs) solve the dynamic equations for the mean (potential) temperature T, salinity S and velocity $\mathbf{U}$:

$$\begin{aligned} &\frac{\partial}{\partial t}(T,S) + U_i\partial_i(T,S) = -\frac{\partial}{\partial x_i}\left(\overline{u_i\theta}, \overline{u_i s}\right) \\ &\frac{\partial U_i}{\partial t} + U_j\partial_j U_i + 2\varepsilon_{ijk}\Omega_j U_k = -\rho_0^{-1}\partial_i P - \frac{\partial}{\partial x_j}\overline{u_i u_j} \end{aligned} \tag{6}$$

Here, θ, s, u_i are the fluctuating components of the temperature, salinity and velocity fields, $\mathbf{\Omega}$ is the Earth's rotation, P is the mean pressure and ε_{ijk} is the totally antisymmetric tensor; overbars denote ensemble averages. To solve Eq. (6), the temperature, salinity and momentum fluxes $\overline{u_i\theta}$, $\overline{u_i s}$, $\overline{u_i u_j}$, representing unresolved processes, must be parameterized in terms of the resolved mean variables T, S, $\mathbf{U}$. In Eq. (6), the mean velocity field is assumed to be incompressible (divergence free) but a treatment of compressible flows is available (Canuto, 1997).

Historically, it was Leonardo da Vinci who, by watching the river Arno in Florence, described the water flow as being made of two distinct parts,[2] which in modern language are called the mean flow and the turbulent, fluctuating component. Several centuries later, Reynolds (1895) suggested splitting the total fields into mean and fluctuating parts, such as $T + \theta$, $S + s$, $\mathbf{U} + \mathbf{u}$, in what has become known as the *Reynolds decomposition*. The non-linear terms in the momentum and temperature (salinity) equations then give rise to the terms on the rhs of Eq. (6). Historically, it took a long time to realize that Eq. (6) were not the last step of the process. By subtracting (6) from the equations for the total fields, one obtains the equations for the fluctuating fields and from them, one proceeds to derive the dynamic equations for the three second-correlations that appear in (6). However, such a suggestion was not made until the twenties by the Russian mathematician A. Friedmann (the same of the expanding universe solution of Einstein's general relativity equations). But, as we shall see in Section 3, even his suggestion was not taken up in a concrete form until 1945 (Chou, 1945). Soon after O. Reynolds' proposal, Boussinesq (1877, 1897, cited in Monin and Yaglom, 1971, vol. I, Section 3) was the first to suggest heuristic, down-gradient type expressions of the form:

$$\overline{w\theta} = -K_h\frac{\partial T}{\partial z}, \quad \overline{ws} = -K_s\frac{\partial S}{\partial z}, \quad \overline{wu} = -K_m\frac{\partial \mathbf{U}}{\partial z} \tag{7}$$

in which $K_{h,s,m}$ represent "turbulent diffusivities". Several comments are needed concerning (7). *First*, even though we have not written out the z-dependence explicitly, each function in (7) is computed at the same z, which means that the model is *local*. Even without knowing the explicit form for the diffusivities (which Boussinesq did not), it is clear that when large eddies are present, as in an unstably stratified, convective region, it is unrealistic to assume that the fluxes at a given z are governed only by what occurs in the vicinity of z since in reality large eddies span much larger extents so large in fact as to be of the same size H of the region, a variable that ought to appear in a non-local version of (7), as we show in Eq. (17).

Stated differently, since by Taylor expansion, to express a non-local function one needs an infinite number of derivatives, taking only the first of them, as in (7), may not be applicable to convective regimes, a topic we shall return to at the end of this section. For the time being, however, we assume that locality is an acceptable approximation since the majority of the ocean is stably stratified

[2] Observe the motion of the water surface, which resembles that of hair, that has two motions: one due to the weight of the shaft, the other to the shape of the curls; thus, water has eddying motions, one part of which is due to the principal current, the other to the random and reverse motion (translated by Prof. U. Piomelli, University of Maryland, private communication, 2008).

and the eddies are correspondingly small. This is likely to be the reason why the relations (7) have been widely used and are amended only when applied to unstably stratified, convective regimes, as discussed in Section 3.

The *second* problem concerns the construction of the diffusivities themselves which we have denoted by K_α. Since diffusivities have dimensions of (length)^2 time^{-1}, on dimensional grounds alone, one has several relations to choose from:

$$K_\alpha \sim \ell^2\tau^{-1} \sim K\tau \sim K^2\varepsilon^{-1} \sim \varepsilon^{1/3}\ell^{4/3} \tag{8}$$

where ℓ is a typical eddy size, K is the eddy kinetic energy, $\tau = 2K\varepsilon^{-1}$ is the dynamical time scale and ε is the rate of dissipation of K. It is important to note that the last relation in (8), which follows from the preceding one using Kolmogorov's law $K \sim \varepsilon^{2/3}\ell^{2/3}$, was actually discovered experimentally by Richardson (1926) 15 years before the appearance of the Kolmogorov's law (Kolmogorov, 1941). However, since contrary to the atmospheric related studies of Richardson in which ℓ represented the separation of two "puffs", in a fully turbulent regime the prescription of ℓ is not straightforward, the most physical representation is the third one that involves K, ε which are calculable quantities for which there exist two dynamic equations, Eq. (20). There is a further reason that can be gleaned from the definitions of K, ε in terms of the spectrum $E(k)$ of the kinetic energy:

$$K = \int E(k)\,dk, \qquad \varepsilon = 2\nu \int k^2 E(k)\,dk \tag{9}$$

These relations show that K's integrand peaks at low wavenumbers (large scales) while ε's peaks at large wavenumbers (small scales) and thus a K–ε representation catches both large and small scales. It may be useful to recall that even though the second relation in (9) contains the kinematic viscosity ν, it is known that ε is independent of it (Frisch, 1995). Postponing the discussion of how to compute K–ε for a moment, we return to (7) and choose the third relation in (8). This gives rise to the two representations (1a) and (1b). The *dimensionless structure functions* S_α that differentiate heat, salt and momentum diffusivities and the *mixing efficiencies* Γ_α, were first introduced in the literature by Mellor and Yamada (1982) and Osborn (1980), respectively. It is quite difficult to guess the structure of S_α and/or Γ_α with any confidence. The reason is rather simple. One must take into account temperature, salinity and velocity or more precisely, their gradients, which are usually represented by the Richardson number Ri and the density ratio R_ρ defined in Eq. (2b). A key task of any mixing scheme is that of constructing the structure functions (2a). In the absence of double diffusion, even without knowing the exact form of (2a), the general dependence on Ri can be guessed at: since shear is a source of mixing, the larger is Ri, the smaller must be the diffusivity. It follows that the structure functions $S_\alpha(Ri)$ must be decreasing functions of Ri. Such general argument is at the basis of the Pacanowski and Philander heuristic model (1981, PP) in which $K_s = K_h$. However, no heuristic structure function has yet been proposed for the momentum diffusivity and in most OGCMs, K_m is treated as a free parameter, e.g., in the GFDL model, it is taken to be $K_m = 1$ cm^2 s^{-1} (Griffies et al., 2005). One could in principle improve on that by using available data on the turbulent Prandtl number (Webster, 1964; Gerz et al., 1989;Schumann and Gerz, 1995; Canuto et al., 2008a, and Fig. 3c):

$$\sigma_t(Ri) = \frac{K_m}{K_h} \tag{10a}$$

and obtain an Ri-dependent K_m using the PP and/or KPP models for K_h with the additional information that at $Ri = 0$, we have (Canuto and Dubovikov, 1996, Eq. (43e)):

$$\sigma_t(Ri = 0) = \frac{Ba}{Ko} = 0.72 \tag{10b}$$

where Ba and Ko (=1.66) are the Batchelor and Kolmogorov constants, respectively.

When double diffusion processes are included, guessing the structure functions (2a) as a function of both Ri and R_ρ using only heuristic arguments is almost impossible, and the only alternative is to adopt the dynamic model known as the Reynolds Stress Model, RSM. After the original work of Chou (1945), within the geophysical context the pioneering work was that of Donaldson (1973) and Mellor and Yamada (1982) who derived the structure functions:

$$S_\alpha(Ri) \tag{11}$$

thus opening the way for non-heuristic derivations of such functions. Since the RSM contains parameters that enter the closure of the pressure correlation terms (a detailed discussion can be found in several papers, e.g., Cheng et al., 2002), the state of the art of turbulent modeling at the time of the MY model was such that the resulting structure functions (11) decreased rapidly with Ri and above a critical Ri(cr) mixing became negligible. Specifically, the MY predicted that:

$$Ri(\mathrm{cr}) = 0.2 \tag{12}$$

a value that three years later Martin (1985) showed to yield too shallow a mixed layer (ML). The same study also showed that in order to reproduce the observed much deeper MLs, a value five times as large was required:

$$Ri(\mathrm{cr}) = O(1) \tag{13}$$

It is fair to say that the apparent inability of the original 1982-MY model to produce "*more mixing*" was a key motivation for the KPP model (Large et al., 1994) which is not based on the RSM but on an analogy with mixing in the atmospheric boundary layer.

In 2001, a mixing scheme using the RSM was proposed (I, listed in Table 1) which showed that (13) can be derived from the RSM, the reason for the difference with (12) being a more complete closure model for the pressure correlations and the ability to compute several of the constants that were poorly known at the time of the MY model but that more recent turbulence modeling allowed to compute, as discussed in I. Thus, the primary achievement of I was to restore "confidence" in the ability of the RSM to yield results in agreement with empirical relations such as (13) by Martin (1985). The model, however, had limitations, the most important of which are (Table 1): (a) the solutions of the RSM equations were rather complex, (b) double diffusion processes were not included, (c) mixing due to tides was missing, and (d) a bottom boundary layer BBL model was not included.

In 2002, a second mixing scheme was proposed (II, listed in Table 1) with the goal to include double diffusion processes while the other parts of the model were the same as in I. The remaining

Table 1
Key features of G1SS mixing schemes.

Mixing scheme	RSM	DD	K–ε	Ri(cr)	Γ: Mixing efficiency	Latitude dependent IGW	Tides	BBL
I, 2001	Complex	No	Local	$O(1)$	Ri	No	No	No
II, 2002	Complex	Yes	Local	R_ρ	Ri, R_ρ	No	No	No
III, present	Simpler	Yes improved	Local	∞	Ri, R_ρ improved	Yes	Yes	Yes

shortcomings of II are therefore: (a) the solutions of the RSM equations are more complex than in I, (b) no mixing due to tides, and (c) no bottom boundary layer.

In 2008, two new features were found which needed to be incorporated into a mixing model: the non-existence of a critical Richardson number (Canuto et al., 2008a) and a better DD model so as to reproduce the measurements of the heat mixing efficiency $\Gamma_h(Ri,R_\rho)$ (Canuto et al., 2008b). Both features are now included in the mixing scheme we present here. In Table 1, we summarize the key features of the models that have been worked out thus far.

Since the additional physical features in III naturally made it more complex, it was necessary to solve the RSM equations so as to obtain a simpler representation of the results than in I, II. Concerning this point, we need to clarify an important issue.

The solutions of the *RSM provide the structure functions* $S_\alpha(Ri,R_\rho)$ *but not the functions* K–ε *which must be computed separately*. This means that in the fourth column in Table 1 one could have used a non-local model for K–ε in any of the three models described thus far, which is how Burchard (2002) carried out extensive studies of models I-II by adopting the structure functions of those models with a non-local model for K–ε.

As already discussed, the fact that the ocean is mostly stably stratified, making locality a legitimate approximation, led us to decide in favor of a local treatment of the K–ε equations. It must, however, be remarked that it is not clear how poorly local models do in an unstably stratified regime such as Deep Convection. For that reason, Canuto et al. (2004a) tested the local K–ε model with the RSM solutions of II in the Labrador Sea and compared the predicted mixed layer depths with both observations and predictions of KPP and MY-2.5 models in which the equation for K is non-local. Comparing the data in Fig. 1 of the paper just cited and the model results displayed in its Figs. 2, 3, 9 and 10a, one concludes that, while all models predict too deep a ML, mixing scheme II in spite of its local nature, performs better than the two non-local models. In addition to the non-locality of the K–ε equations, there is an equally important missing feature, mixed layer mesoscales and sub-mesoscales that are known to re-stratify the ML leading to a shallower ML, as we discuss in the Conclusions. At this point, it is therefore not entirely clear to us how physically relevant is the local vs. non-local nature of the vertical mixing model, a feature we plan to study in the future.

3. Structure of the new mixing scheme

In describing the new parameterization, we follow the items as they appear in Table 1, fourth row, from left to right. We begin with the RSM, Reynolds Stress Model which, as already mentioned, has a long history whose first application to shear flows appeared in 1945 (Chou, 1945). For discussions of the RSM, especially in geophysical problems, we suggest the pioneering work of Donaldson (1973) and Mellor and Yamada (1982), and the recent reviews by Burchard (2002), Cheng et al. (2002) and Umlauf and Burchard (2005). The work of Donaldson (1973) is particularly relevant not only for its extensive discussion of the closure of higher-order moments in terms of lower-order ones, but because it is the first time that "four basic principles" were presented in Section 8.4 of Donaldson (1973) which we briefly enumerate: (1) the model must be written in covariant or tensor form (so as to be invariant under arbitrary transformation of coordinate systems), (2) the model must be invariant under a Galilean transformation, (3) the model must have the dimensional properties of the term it replaces, and (4) the model must satisfy all the conservation properties characterizing the variables in question. How these principles helped the closure problem is elucidated by several instructive examples in the same Section 8.4.

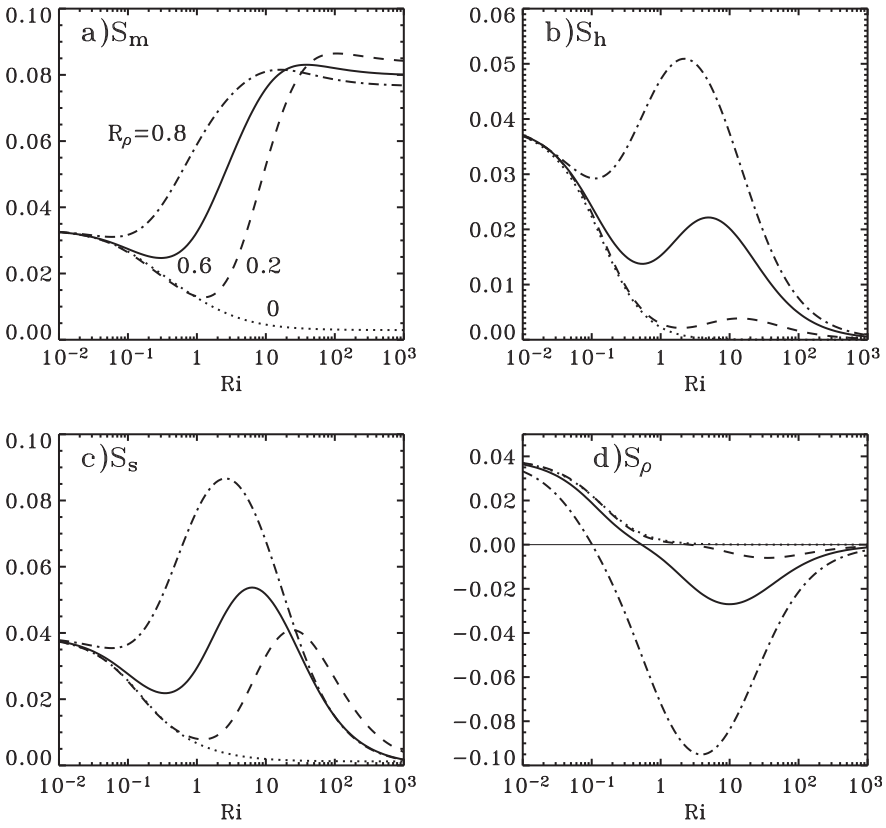

Fig. 1. The structure functions S_α for momentum, heat, salt and density, see Eqs. (1a), (30)–(41) and (55) are plotted vs. Ri for different R_ρ.

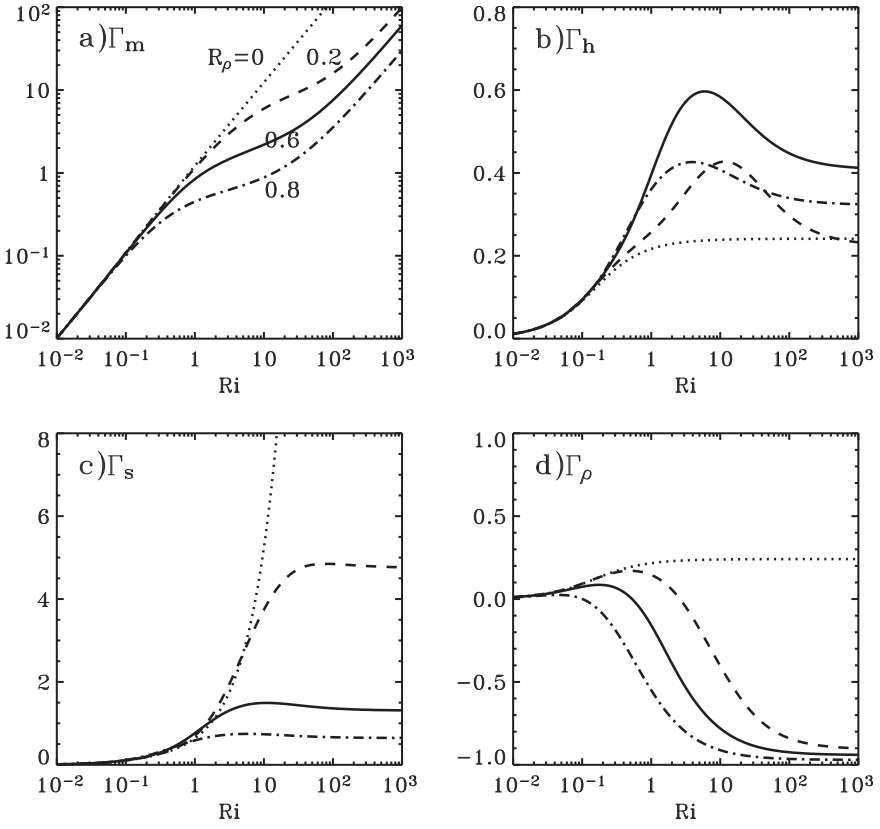

Fig. 2. Same as Fig. 1 but for the mixing efficiencies Γ_α defined in Eq. (1b).

3.1. Local and non-local RSM equations

Though the mean equations (6) require only the fluxes of heat, salt and momentum:

$$\overline{w\theta}\ \text{(heat flux)},\quad \overline{ws}\ \text{(salt flux)},\quad \overline{u_iu_j} = \tau_{ij}\ \text{(Reynolds stresses)} \tag{14a}$$

the dynamic equations of the variables (14a) involve three more correlations (see Appendix A):

$$\overline{\theta^2}\ \text{(temp. variance)},\quad \overline{s^2}\ \text{(salin. variance)},\quad \overline{\theta s}\ \text{(temp.-salin. correlation)} \tag{14b}$$

For completeness, we present a brief, hopefully illustrative, example of how the RSM equations are derived. One begins with the Reynolds decomposition whereby the full velocity and temperature fields are written as the sum of a mean and a fluctuating part, $\mathbf{U}+\mathbf{u}$, $T+\theta$; next, one averages the resulting equations using $\bar{\mathbf{u}}=0, \bar{\theta}=0$ and subtracts the results from the original equations for the total fields. The results of this purely algebraic procedure are the equations for the fluctuating $\mathbf{u},\theta$ fields that read as follows:

$$\begin{aligned}\frac{Du_i}{Dt}+\frac{\partial}{\partial x_j}\left(u_iu_j-\overline{u_iu_j}\right) &= -\frac{\partial p}{\partial x_i}-u_jU_{i,j}+\alpha_T g_i\theta+\nu\frac{\partial^2 u_i}{\partial x_i^2}\\ \frac{D\theta}{Dt}+\frac{\partial}{\partial x_i}\left(u_i\theta-\overline{u_i\theta}\right) &= -u_iT_{,i}+\kappa_T\frac{\partial^2\theta}{\partial x_i^2}\end{aligned} \tag{15}$$

where κ_T is the thermometric diffusivity and ν/κ_T is the molecular Prandtl number ($\approx$7 for seawater). Since each fluctuating variable has zero average, averaging Eq. (15) yields an identity 0 = 0. To obtain the equations for the second-order moments (14), one proceeds as follows: multiply the first of (15) by θ and the second by u_i and add the two; the result is the equation for the heat flux $\overline{u_i\theta}$. Multiplying the second of (15) by θ, one obtains the equation for the temperature variance and so on. The physical difficulty, known as the *closure problem*, is represented by the third-order moments,[3] TOMs, such as $\overline{p_{,i}\theta}$, $\overline{p_{,i}u_j}$ and $\overline{u_iu_ju_k}$, $\overline{u_iu_j\theta}$, $\overline{u_i\theta^2}$ which physically represent the fluxes of Reynolds stresses, heat fluxes and temperature variance that must also be "closed", that is, parameterized in terms of the second-order moments. How this is done was discussed in detail in Canuto (1992) and more recently in Cheng et al. (2002, 2005) and there is therefore no need to repeat the discussion here. However, what must be stressed is the *non-local effects* represented by the TOMs. The point is that turbulence not only gives rise to non-zero second-order correlations but it also transports them around, that being the meaning, for example, of the term $\overline{u_iu_j\theta}$ that represents the flux of "heat fluxes". Similar interpretations apply to the other TOMs. When such transport processes are included, one has a non-local model since even if the local gradients are zero at some point, implying a zero flux and no mixing on the basis of (7), the non-local terms ensure the existence of mixing brought about by the fluxes just discussed. To give a concrete and simple example, consider the equation for the temperature variance obtained from the second of (15). Using the closure $\kappa_T\overline{\theta\theta}_{,ii}=-\overline{\theta^2}/\tau_\theta$ that was derived and justified in the papers just cited, one obtains in the 1D and stationary limits:

$$\overline{\theta^2}=-\tau_\theta\overline{w\theta}\frac{\partial T}{\partial z}-\frac{1}{2}\tau_\theta\frac{\partial}{\partial z}\overline{w\theta^2} \tag{16}$$

This shows that where the mean temperature gradient is zero, the temperature variance does not vanish due to the flux of $\overline{\theta^2}$

[3] Along a streamline of an inviscid fluid one has (Euler's law) $\frac{1}{2}\rho\partial u^2/\partial\ell=-\partial p/\partial\ell$ which leads to $\frac{1}{2}\rho u^2+p=$ const. which shows that the pressure is a second-order moment.

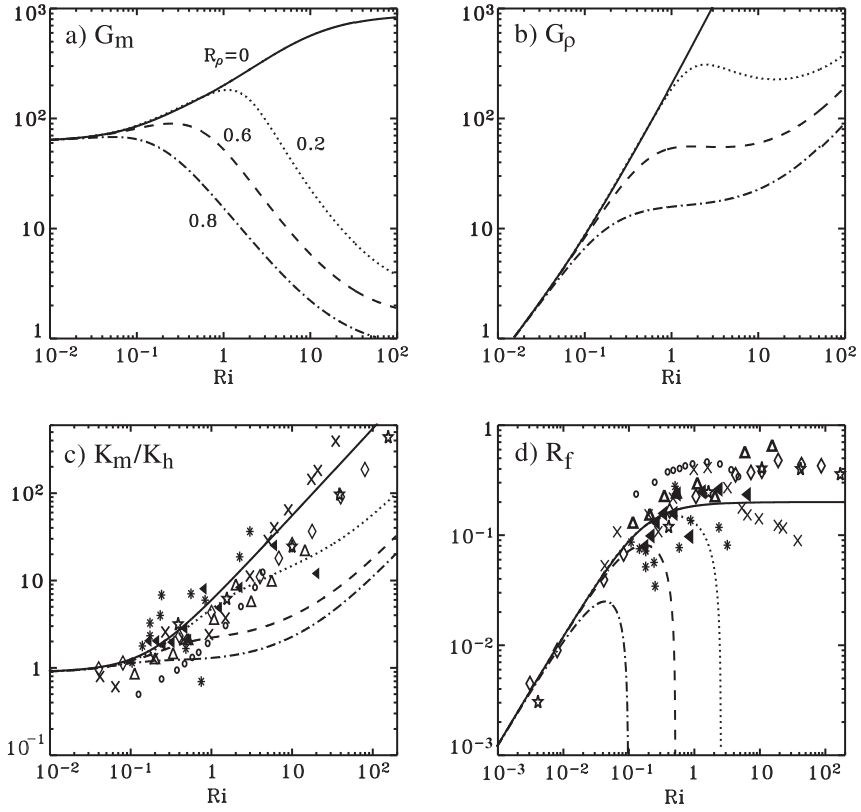

Fig. 3. (a) Dynamical eddy turnover time $\tau = 2K/\varepsilon$, specifically, $G_m = (\tau\Sigma)^2$ vs. *Ri* for different R_ρ solution of Eq. (41); (b) same as in (a) but for the turnover time, specifically, $G_\rho = (\tau N)^2$, with the inclusion of double diffusion processes, see Eqs. (26) and (27); (c) turbulent Prandtl number defined in Eqs. (10) with the effect of DD; (d) flux Richardson number defined in Eq. (42) with the effects of DD. In panels (c) and (d) the data correspond to the case without DD processes: Kondo et al. (1978, slanting black triangles), Bertin et al. (1997, snow-flakes), Strang and Fernando (2001, black circles), Rehmann and Koseff (2004, slanting crosses), Ohya (2001, diamonds), Zilitinkevich et al. (2007, 2008 LES, triangles), (Stretch et al., 2001, DNS, five-pointed stars).

represented by the second, non-local, term. Deardorff (1966) parameterized non-locality by adding a *counter-gradient term* γ_h:

$$J \equiv \overline{w\theta} = -K_h \frac{\partial T}{\partial z} + \gamma_h, \qquad \gamma_h \sim \tau_\theta \frac{\partial \overline{w\theta^2}}{\partial z} \sim \tau H^{-1} w_* J_* \tag{17}$$

where the "closure" of γ_h proposed by Holtslag and Moeng (1991) is a simplified form of the z-derivative of $\overline{w\theta^2}$ but one that exhibits an essential feature, the extent H which represents, as we discussed earlier, the fact that when eddies are as large as the "container", the size of H ought to appear in the equations (* represent fiducial values). We have also taken $\tau_\theta \sim \tau \sim K/\varepsilon$. It must be stressed that it would be unjustified to adopt the same form (17) of the counter-gradient also for the salinity and/or momentum fluxes whose form requires modeling the corresponding TOMs, an active field of research, as discussed in a recent work (Cheng et al., 2005).

The problem of how to solve the RSM equations for the second-order correlations (14), including the non-local terms, was studied in a recent paper (Canuto et al., 2005) where it was shown how to write the fluxes as the sum of local and non-local terms, see for example Eq. (9a) of the cited paper. The strategy here is that of first solving the local limits of the RSM equations and then adding the non-local TOMs terms once a closure form has been chosen. However, since the closure of the TOMs is still an active field of research, it would be premature to adopt any particular closure now.

3.2. Ri and R_ρ dependence of the RSM solutions

The structure functions derived in paper II, Eqs. (13a)–(15), depend on three variables:

$$S_\alpha = S_\alpha\left[(\tau N)^2, R_\rho, (\tau\Sigma)^2\right] \tag{18}$$

Since in general, N^2 and Σ^2 appear separately and not as their ratio *Ri*, Eq. (18) does not exhibit the form (5) which entails only two large scale variables, *Ri* and R_ρ. This dissimilarity between (5) needs some comments. First, even if we rewrite (18) in the equivalent form:

$$S_\alpha = S_\alpha\left[Ri, R_\rho, (\tau\Sigma)^2\right] \tag{19}$$

the function $(\tau\Sigma)^2$ still depends on turbulence via the dynamical time scale τ and therefore at the level of (18) and (19), the problem is not "closed". At this point, one has two choices.

The *first choice is to adopt a non-local K–ε model* (for a detailed discussion of the *K*–ε model, its applications and the ε-equation, see Pope (2000, Section 10.4) and Burchard (2002)):

$$\frac{DK}{Dt} + \frac{\partial F_K}{\partial z} = P - \varepsilon, \quad \frac{D\varepsilon}{Dt} + \frac{\partial F_\varepsilon}{\partial z} = \frac{\varepsilon}{K}(c_1 P_m + c_3 P_b - c_2\varepsilon) \tag{20}$$

where $c_{1,2} = 1.44, 1.92$ and $F_{K,\varepsilon}$ are the TOMs representing the fluxes of *K* and ε:

$$F_K = \frac{1}{2}\overline{wu_i u_i}, \qquad F_\varepsilon = \overline{w\varepsilon} \tag{21}$$

while the buoyancy and shear production terms are defined as follows:

$$P_b = g(\alpha_T \overline{w\theta} - \alpha_s \overline{ws}) = -g\alpha_T \frac{\partial T}{\partial z}(K_h - K_s R_\rho) \tag{22}$$

$$P_m = -(\overline{uw}U_z + \overline{vw}V_z) = K_m \Sigma^2 \tag{23}$$

The sign and magnitude of the coefficient c_3 in Eq. (20) are discussed in Burchard (2002). In writing (23), we have anticipated the fact, to be proven shortly below, that the solutions of the RSM are indeed of the form (7). Once a closure for (21) is chosen, the solutions of (20) yield K and ε and thus $\tau = 2K/\varepsilon$. This was the procedure used by Burchard (2002) in the 1D-GOTM ocean model in which the following closure for the TOMs was adopted:

$$F_K = -K_m \frac{\partial K}{\partial z}, \quad F_\varepsilon = -\sigma_t^{-1} K_m \frac{\partial \varepsilon}{\partial z} \tag{24}$$

To our knowledge, Eq. (20) have not yet been used in 3D global OGCMs. The French 3D ocean code OPA employs the first of Eq. (20) and a heuristic representation of ε in lieu of the second equation in (20).

The *second choice is to adopt a stationary, local model for K*:

$$P = \varepsilon, \quad \text{production} = \text{dissipation} \tag{25}$$

and a model for ε, as discussed in Section 6. Anticipating that the RSM does give rise to diffusivities of the form (1), $P = \varepsilon$ becomes the following algebraic relation:

$$P = \varepsilon: \qquad \frac{1}{2}(\tau\Sigma)^2 S_m - \frac{1}{2}(\tau N)^2 S_\rho = 1 \tag{26}$$

where:

$$S_\rho = \frac{S_h - S_s R_\rho}{1 - R_\rho} \tag{27}$$

Using Eq. (19), the solution of (26) yields the desired relation (4):

$$(\tau\Sigma)^2 = f(Ri, R_\rho) \tag{28}$$

and thus the final form of (19) is:

$$S_\alpha = S_\alpha(Ri, R_\rho) \tag{29}$$

which coincides with Eq. (5), thus explaining the conditions of validity of the latter. The explicit form of (28) is obtained by solving Eqs. (40) and (41). Of course, after determining τ we still need a model for ε which is discussed in Section 6.

3.3. New strategy for the solution of the RSM

The RSM equations (5)–(11) of paper II are presented in Appendix A for several reasons:

(1) to make this paper self-contained,
(2) to correct misprints in II, specifically, Eqs. (5) and (9),
(3) to give directly the 1D form which is the one being solved (using also a simplified notation $\overline{w''T''} \to \overline{w\theta}$, $\overline{T''^2} \to \overline{\theta^2}$, $\overline{w''s''} \to \overline{ws}$, $\overline{s''^2} \to \overline{s^2}$, $\overline{T''s''} \to \overline{\theta s}$),
(4) Eq. (5, II) for the Reynolds stress can be considerably simplified by dropping the second term on the rhs of it since the coefficient p_1 is very close to unity, and by rounding off the value of p_2 to 1/2. The p_1 term added much complexity to the solution and yet its contribution was quite small. As a result, Eq. (A.6) is simpler than Eq. (5, II) and yet it preserves the key physical ingredients,
(5) in paper II, we employed a method of symbolic algebra to solve Eqs. (5–11, II) simultaneously. The resulting structure functions Eqs. (13a–15, II) were algebraic but cumbersome. However, inspection of the 1D form given in Appendix A reveals that this was not an optimal choice since the first five equations do not depend on shear which appears only in Eq. (A.6). Thus, one can separate the problem into two parts: first, one solves Eqs. (A.1)–(A.5) analytically (without the need of symbolic algebra methods) and in a second step, one solves Eqs. (A.6)–(A.10) for $\overline{w^2}$. This simple observation has allowed us to obtain solutions that are considerably simpler than those in paper II.

4. Explicit form of the new mixing scheme

4.1. Heat and salt diffusivities

The analytic solutions of Eqs. (A.1)–(A.5) yield the following form of the dimensionless structure functions:

$$S_{h,s} = A_{h,s} \frac{\overline{w^2}}{K} \tag{30}$$

where:

$$A_h = \pi_4 \left[1 + px + \pi_4\pi_2 x\left(1 - r^{-1}\right)\right]^{-1}, \quad A_s = A_h (rR_\rho)^{-1} \tag{31}$$

Following standard notation, we denote by r the heat-to-salt flux ratio given by the following relations:

$$r \equiv \frac{\alpha_T \overline{w\theta}}{\alpha_s \overline{ws}} = \frac{1}{R_\rho}\frac{K_h}{K_s}, \qquad \frac{K_h}{K_s} = \frac{\pi_4}{\pi_1}\frac{1 + qx}{1 + px} \tag{32}$$

where the dimensionless variables x, p and q are defined as follows:

$$x = (\tau N)^2 \left(1 - R_\rho\right)^{-1}, \quad p = \pi_4\pi_5 - \pi_4\pi_2\left(1 + R_\rho\right),$$
$$q = \pi_1\pi_2\left(1 + R_\rho\right) - \pi_1\pi_3 R_\rho \tag{33}$$

The π_k's are the dissipation - relaxation time scales defined in Eq. (12) of II made dimensionless by using the dynamical time scale $\tau = 2K/\varepsilon$. As one can observe, the fact that we have not yet used Eq. (A.6) for the Reynolds stresses is manifest in the still unknown $\overline{w^2}/K$ term in (30) which we determine next.

4.2. Momentum diffusivity

Consider the Reynolds stress equations (A.6)–(A.10). In the stationary limit, one obtains a set of linear algebraic equations in the variable b_{ij} which can be solved. The structure functions for the case of momentum have the following form:

$$S_m = A_m \frac{\overline{w^2}}{K}, \quad A_m = \frac{A_{m1}}{A_{m2}} \tag{34}$$

where:

$$A_{m1} = \frac{4}{5} - \left[\pi_4 - \pi_1 + \left(\pi_1 - \frac{1}{150}\right)\left(1 - r^{-1}\right)\right] x A_h \tag{35}$$

$$A_{m2} = 10 + \left(\pi_4 - \pi_1 R_\rho\right)x + \frac{1}{50}(\tau\Sigma)^2 \tag{36}$$

4.3. The ratio $\overline{w^2}/K$

The general form of the ratio $\overline{w^2}/K$ is given by:

$$\frac{\overline{w^2}}{K} = \frac{2}{3}\left[1 + \frac{2}{15}X + \frac{1}{10}A_m(\tau\Sigma)^2\right]^{-1}, \quad X \equiv \left(1 - r^{-1}\right)x A_h \tag{37}$$

It is important to note that, contrary to what has been done in many ocean models, it is no longer necessary to guess the momentum diffusivity, as discussed in Section 1, since the model provides K_m as it provides heat and salt diffusivities. In conclusion, the above formulation shows that all the variables exhibit the dependence on the three functions:

$$(\tau N)^2, (\tau\Sigma)^2, R_\rho \to Ri, R_\rho, (\tau\Sigma)^2 \tag{38}$$

4.4. Dynamical time scale τ

If one solves Eq. (20) for K and ε, $\tau = 2K/\varepsilon$ is automatically given as a function of Ri and R_ρ. If, on the other hand, one uses the local model represented by the assumption $P = \varepsilon$, simplifications of the above equations are possible. Expressions (31) for $A_{h,s}$ remain the same while expressions (35)–(37) simplify to:

$$A_m = \frac{2}{(\tau\Sigma)^2}\left(\frac{15}{7}+X\right), \quad \frac{1}{2}\frac{\overline{w^2}}{K} = \left(\frac{30}{7}+X\right)^{-1} \tag{39}$$

Next, using the notation by Mellor and Yamada (1982):

$$G_m \equiv (\tau\Sigma)^2 \tag{40}$$

Eq. (26) becomes a cubic equation for G_m in terms of Ri and R_ρ:

$$\begin{aligned} &c_3 G_m^3 + c_2 G_m^2 + c_1 G_m + 1 = 0 \\ &c_3 = A_1 Ri^3 + A_2 Ri^2, \quad c_2 = A_3 Ri^2 + A_4 Ri, \quad c_1 = A_5 Ri + A_6 \end{aligned} \tag{41}$$

The functions A_k's are given in Appendix B, Eqs. (B.12). Once the function $G_m(Ri,R_\rho)$ is known, one can construct all the relevant functions the most prominent of which, the structure functions, are presented in Fig. 1, the mixing efficiencies in Fig. 2 and the time scales in Fig. 3a and b. For example, Fig. 3a exhibits several new features; in mixing model II with a finite Ri(cr), the function G_m became infinitely large at $Ri(\mathrm{cr}) = O(1)$ corresponding to the vanishing of the eddy kinetic energy since $\tau \sim \ell K^{-1/2}$, which is the way Ri(cr) was defined in that scheme. An alternative interpretation is that at Ri(cr), the eddy lifetime becomes very large indicating a tendency toward laminarity, that is, in the absence of the breakups of the linear structures by the non-linear interactions, the eddy life times $\tau \to \infty$. In the present mixing scheme with no Ri(cr), in the case without DD processes $R_\rho = 0$, G_m still increases as Ri increases and turbulence decreases but it no longer diverges at any Ri reaching instead a finite asymptotic value. However, in the presence of DD processes and at sufficiently large Ri corresponding to a vanishing shear (a source of mixing), the DD itself becomes a source of mixing which leads to a decrease of the eddy life time and G_m decreases correspondingly. On the other hand, the results also show that as long as shear is strong (small Ri), DD has no effect being overpowered by the stronger action of shear and thus all R_ρ give the same result as $R_\rho = 0$. It is known from laboratory data (Linden, 1971) that strong shear disrupts salt finger formation. As the data presented in Figs. 9 and 10 of Canuto et al. (2008a) show, the lack of an Ri(cr) is more evident in the momentum than in the heat flux which becomes very small at $Ri > O(1)$ and that is why the function $G_\rho \equiv (\tau N)^2$ in Fig. 3b still grows with Ri when DD processes are not present ($R_\rho = 0$), and why the presence of DD processes softens the growth but does not have nearly as dramatic an effect as in Fig. 3a.

In Fig. 3c we present the turbulent Prandtl number, Eq. (10), vs. Ri. We have superimposed data for the no-DD case to show that the model reproduces them satisfactorily. Finally, in Fig. 3d we plot the flux Richardson number derived from Eqs. (22), (23), (27) and (32):

$$P = K_m\Sigma^2(1-R_f), \quad R_f = Ri\frac{K_\rho}{K_m} = Ri\frac{K_h}{K_m}\frac{1-r^{-1}}{1-R_\rho} \tag{42}$$

For the $R_\rho = 0$ no-DD case, the available data are well reproduced since $(1-r^{-1})(1-R_\rho)^{-1}$ is unity in this case. DD processes affect R_f quite significantly: in the strongest DD case considered here, $R_\rho = 0.8$, R_f becomes negative quite early. The physical interpretation of $R_f < 0$ is that the buoyancy flux, instead of acting like a sink as in the absence of DD processes, becomes a source of mixing due to salt fingers instabilities and contributes positively to the total production P.

4.5. Overview

The mixing model is now complete since momentum, heat and salt diffusivities have been expressed in terms of the resolved fields represented by two large scale variables Ri and R_ρ, and Eq. (6) can therefore be solved.

5. Tests of the mixing model without an OGCM

Before using the above mixing model in an OGCM, we believe it is important to assess its validity and predictions without using an OGCM. In what follows, we present the tests we have carried out.

5.1. Test: strong shear

Since x defined in Eq. (33) represents the eddy turnover time τ, a strong turbulent regime ($Ri \ll 1$) corresponds to small τ's and a small x, in which case the last relation in Eq. (32), together with Eq. (A.11), yields:

$$K_h = K_s \tag{43}$$

which is a reassuring result since when mixing is strong, such as in the ocean's wind driven mixed layer, there is no difference between salt and heat diffusivities, as it was proven in laboratory experiments (Linden, 1971). Double Diffusion processes can only operate when shear has subsided, which occurs below the ML.

5.2. Test: weak shear

This case corresponds to neglecting shear in (26). Using (32) and (33), Eq. (26) acquires the form:

$$\frac{1}{2}(\tau N)^2 S_h = (1-R_\rho)(r^{-1}-1)^{-1} \tag{44}$$

Using the representation (1b), that is:

$$K_\alpha = \Gamma_\alpha \frac{\varepsilon}{N^2}, \quad \Gamma_\alpha \equiv \frac{1}{2}(\tau N)^2 S_\alpha \tag{45}$$

and combining Eqs. (44) and (45), the mixing efficiency for the temperature field is given by:

$$\Gamma_h = (1-R_\rho)(r^{-1}-1)^{-1} \tag{46}$$

In the case of salt fingers, measured data give $r \approx 0.6$–0.7, $R_\rho \approx 0.6$–0.7 (Kunze, 2003; Schmitt, 2003) and thus the model predicts that Γ_h has the value:

$$\Gamma_h = 0.6\text{—}0.7 \tag{47}$$

in agreement with the last panel in Fig. 4. We also note that (47) is more than 3 times larger than the canonical 0.2 with no double diffusion (Osborn, 1980, Eq. (10)).

5.3. Test: onset of salt fingers at R_ρ(cr)

Next, we assess the model ability to predict the value of R_ρ(cr) that characterizes the onset of salt fingers (SF) and diffusive convection (DC). It is important to recall that linear analysis predicts that SF occur in the regime (Schmitt, 1994):

$$\frac{\kappa_s}{\kappa_T} \simeq 10^{-2} \leqslant R_\rho \leqslant 1 \tag{48}$$

where the lhs is the ratio of the salt to heat kinematic molecular diffusivities. On the other hand, Schmitt and Evans (1978) showed that in the ocean SF become strongly established when:

$$R_\rho \geqslant R_\rho(\mathrm{cr}) \approx 0.6 \tag{49}$$

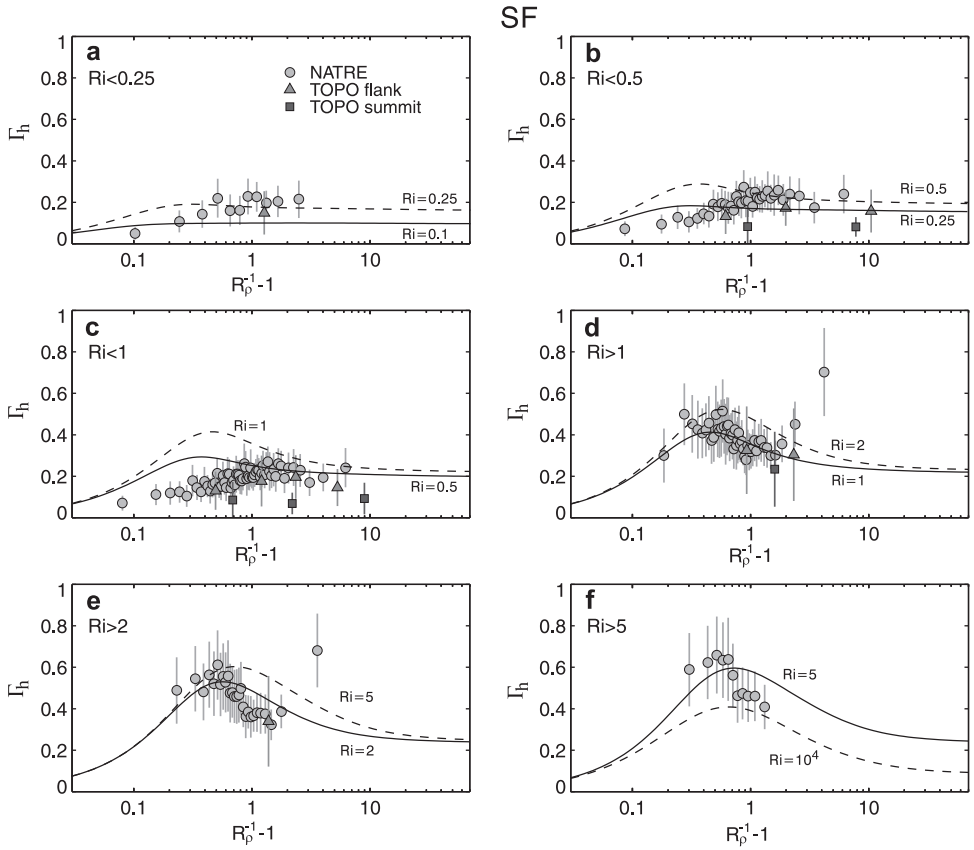

Fig. 4. The heat mixing efficiency $\Gamma_h(Ri,R_\rho)$ defined in Eq. (1b). The model results (dashes and full lines) are superimposed on the data from NATRE-TOPO from St. Laurent and Schmitt (1999, Fig. 9).

which is quite different than (48). First, we comment on the fact that the present model is sufficiently general to encompass (48) in the appropriate limit and then show that it does yield the correct result (49). The present RSM formalism is valid for arbitrary dissipation-relaxation time scales that appear in the last terms in Eqs. (A1)–(A5) and (A9) and (A10) and which, when written in units of the dynamical time scale τ, are denoted by the π's which in general depend on both the kinematic molecular heat, salt and momentum diffusivities, a well as on Ri and R_ρ. Relations (A.11) used here correspond to relatively large Reynolds numbers Re. In the limit of small Re, the form of the π's was given by Zeman and Lumley (1982) and when used in (32), it yields (48). In spite of several attempts, we have not yet been able to find a general expression for the π's valid for all Re. To show that the present large Re model yields a value corresponding to (49), we consider Fig. 2b which represents the heat mixing efficiency Γ_h vs. Ri for different R_ρ. The interesting feature is that as one begins with $R_\rho = 0$ and increases its value, there is an uppermost curve past which a further increase in R_ρ corresponds to lower values of Γ_h. The R_ρ value corresponding to the maximum Γ_h, which we shall call $R_\rho(\mathrm{cr})$, can be read from the curves to be around:

$$R_\rho(\mathrm{cr}) \approx 0.6 \tag{50}$$

which reproduces (49) corresponding to the onset of SF.

5.4. Test: mixing efficiency Γ_h

Using NATRE and TOPO data to estimate χ (rate of dissipation of the temperature variance) and ε, SS99 plotted the heat mixing efficiency Γ_h (Oakey, 1985) as a function of Ri and R_ρ:

$$\Gamma_h = \frac{1}{2}\frac{\chi}{\varepsilon}\frac{N^2}{(\partial T/\partial z)^2} \tag{51}$$

Let us note that (51) corresponds to the stationary limit of Eq. (A.3) where $\chi = 2\overline{\theta^2}\tau_\theta^{-1}$, with $\tau_\theta = \tau\pi_5$. SS99 results, shown in Fig. 4, exhibit new and interesting features, the most prominent of which is the fact that the canonical value $\Gamma_h = 0.2$ which has been used for years, is valid only in the presence of strong shear when double diffusion (DD) processes cannot operate. However, when shear subsides and DD become active, the mixing efficiency becomes 3–4 times as large (Fig. 4f).

The challenge for any mixing scheme is to reproduce the data of Fig. 4. We begin by showing that Eq. (4) of SS99 (we recall that $R_\rho(\mathrm{SS99}) \equiv R_\rho^{-1}$):

$$\Gamma_h = \frac{R_f}{1-R_f}\frac{1-R_\rho}{1-r^{-1}} \tag{52}$$

is identical to our Eq. (1b) under $P = \epsilon$. First, the flux Richardson number, including double diffusion processes, is defined as:

$$R_f = \frac{K_\rho}{K_m}Ri = \frac{\Gamma_\rho}{1+\Gamma_\rho} \tag{53}$$

The buoyancy diffusivity K_ρ follows from (22) rewritten as:

$$P_b = -g\alpha_T\frac{\partial T}{\partial z}(K_h - K_s R_\rho) = -K_\rho N^2 \tag{54}$$

where K_ρ is the mass diffusivity given by:

$$K_\rho = K_h(1-r^{-1})(1-R_\rho)^{-1} \tag{55}$$

This allows us to write the total production P in the compact form:

$$P = K_m\Sigma^2 - K_\rho N^2 \tag{56}$$

Eliminating K_m between (53) and (56), the form of Γ_h given in (52) becomes:

$$\Gamma_h = \frac{N^2}{\varepsilon}K_h = \frac{1}{2}(\tau\Sigma)^2 RiS_h \tag{57}$$

which is Eq. (1b). The model predictions based on Eq. (57) are plotted in Fig. 4. The model reproduces the major features of the SS99 data.

To put the model results of Fig. 4 in perspective, we point out that to the best of our knowledge, no mixing model has thus far reproduced these data. In fact, all treatments we have seen employ a heat mixing efficiency of 0.2 irrespectively of whether there are DD processes or not. It is perhaps more accurate to say that they neglect DD and in so doing, they underestimate the true mixing which, as demonstrated in Fig. 4f, can be up to three times as large as the No-DD case.

5.5. Test: low and high ε-modes

SS99 analysis of the NATRE data further revealed a bimodal distribution of the kinetic energy dissipation rate ε. The first regime, called the high ε-mode, is characterized by a dissipation rate of the order of 10^{-9} W/kg, while the second regime, called the low ε-mode, is characterized by values 10 times smaller than those of the first mode, $\varepsilon = 0.1 \times 10^{-9}$ W/kg. The first mode was identified with an $Ri < 1$ turbulent regime while the latter was identified with an $Ri > 1$, salt finger dominated regime. The challenge posed by these data to any mixing model is not trivial. The reason is that the latter usually do not include dynamic equations for the dissipation variables ε, χ which in SS99 were taken from the data themselves. An heuristic equation for ε exists, second of Eq. (20) but lacks double diffusion, thus making the second of (20) too incomplete for the case under study. We therefore suggest the following alternative. Using Eq. (51), we derive the following relation:

$$\varepsilon = \frac{1}{4}C\frac{(1-R_\rho)^2}{N_*^2\Gamma_h} \quad (10^{-9}\,\mathrm{W/kg}) \tag{58}$$

where we have used the following notation: $N_*^2 = N^2/N^2_{\mathrm{NATRE}}$, $N^2_{\mathrm{NATRE}} = 1.7 \times 10^{-5}\ \mathrm{s}^{-2}$, $C = \chi_9\alpha_3^2$, $\chi_9 = \chi/10^{-9}\ \mathrm{K}^2\ \mathrm{s}^{-1}$ and $\alpha_3 = \alpha_T/(3 \times 10^{-4}\ \mathrm{K}^{-1})$. Using the mixing model result shown in Fig. 4 for the mixing efficiency Γ_h, in Fig. 5a we plot relation (58) for the NATRE case corresponding to $C = 1$ and $N_*^2 = 1$. From the figure we deduce that:

$$\varepsilon(Ri = 0.05) = 10\varepsilon(Ri = 10) \tag{59}$$

a result in general agreement with the SS99 finding. It must be noted, however, that contrary to the case of the mixing efficiency $\Gamma_h(Ri,R_\rho)$ for which the mixing model provided the full function $\Gamma_h(Ri,R_\rho)$ which we compared directly with the data, in relation (58) the uncertainties still present in modeling χ are such that the mixing model is unable to provide the full function $\varepsilon(Ri,R_\rho)$. To arrive at the results presented in Fig. 5a, we borrowed the function χ from the SS99 data. Regrettably, at this stage of model development, we cannot do any better.

5.6. Test: heat to salt flux ratio $r(Ri,\rho)$

In the $Ri \gg 1$ case, the heat to salt flux ratio is given by Eq. (46) which we rewrite as:

$$r = \frac{\Gamma_h}{1 + \Gamma_h - R_\rho} \tag{60}$$

which depends on the mixing efficiency $\Gamma_h(Ri,R_\rho)$ which we have already assessed in Fig. 4. Eq. (60) is plotted in Fig. 5b together with the data of Fig. 10a of SS99. The SS99 data, represented by the blue line and the gray area representing the errors, are satisfactorily reproduced by the model.

5.7. Test: momentum diffusivity and turbulent Prandtl number

The turbulent Prandtl number, given by Eqs. (10), (1) and (30)–(37), is shown in Fig. 3c. In most OGCMs, the momentum diffusivity K_m is treated as a free parameter with a value frequently taken to be 10 times larger than K_h, that is, 1 $\mathrm{cm}^2\ \mathrm{s}^{-1}$, which means a turbulent Prandtl number of 10 which corresponds to an $Ri = 2$–4, as shown in Fig. 3c, which is larger than the value corresponding to the internal gravity waves field, as discussed in Section 7.2.

5.8. Previous models

In paper II, we reviewed some previous models and here we need to update the discussion. We begin with the work of Smyth and Kimura (2007) who employed linear stability analysis to study DD under the influence of shear. When they compared the model results for Γ_h with the data of Fig. 4, the predicted dependence on R_ρ was the opposite to that of the data. Inoue et al. (2007)

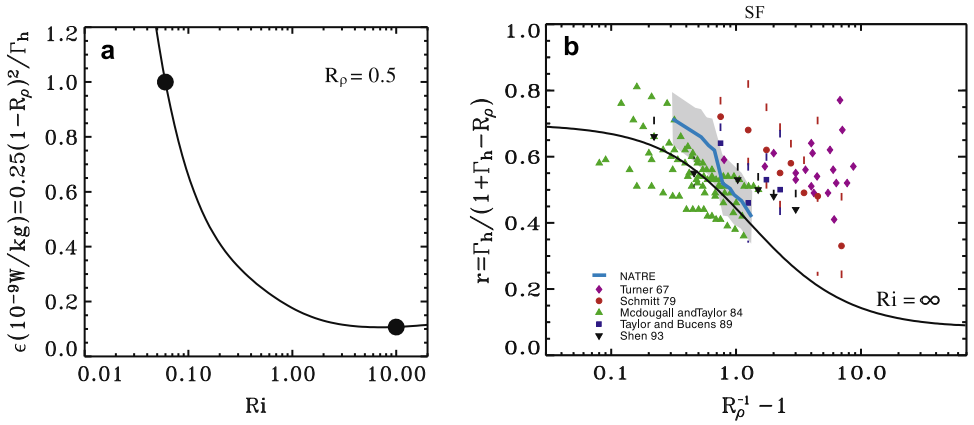

Fig. 5. (a) Plot of the kinetic energy dissipation ε in units of 10^{-9} W/kg given by Eq. (58) vs. Ri for $R_\rho = 0.5$; the two values at $Ri = 0.05$ and 10 yield a ratio of 10 which is in accord with the SS99 finding of a bimodal distribution of the kinetic energy dissipation; (b) plot of the heat to salt flux ratio $r(Ri,R_\rho)$ given by Eq. (60), for vanishing shear. The NATRE data of SS99 are indicated by the blue line with the gray area indicating the error bars. The model reproduces the data satisfactorily. (For interpretation of the references in color in this figure legend, the reader is referred to the web version of this article.)

employed a model similar in spirit to the partition first suggested by Walsh and Ruddick (2000) which reads:

$$K_\alpha(Ri, R_\rho) = \underbrace{K_\alpha(Ri > 1, R_\rho)}_{\text{DD}} + \underbrace{K_\alpha(Ri < 1)}_{\text{Turb}} \tag{61}$$

with the understanding that the turbulent part no longer depends on the density ratio R_ρ. Since the ratio K(turb)/K(DD) is not given by the WR model, it was treated as a free parameter. Inoue et al. (2007) defined the crossing point when the Reynolds number Re = $\varepsilon(\nu N^2)^{-1} = 20$; they further employed a heuristic expression for the salt diffusivity K_s in the SF regime suggested by Zhang and Huang (1998) while for K_h they employed the first of (32) with a constant $r = 0.71$. For the DC regime, they employed a model for K_h and r suggested by Kelley (1990). However, as none of their relations contains Ri, it seems unlikely that they can reproduce the data in Fig. 4.

As for coupled global oceanic-atmospheric codes, the GFDL code (Griffies et al., 2005, see their Eqs. (2)–(4)) accounts for SF but not DC and employs laboratory data to model SF. However, since there is no Ri dependence in such DD model, the resulting heat mixing efficiency may be underestimated when SF processes are strong.

We complete the discussion about DD with some brief remarks about their oceanic importance (Ruddick and Gargett, 2003). WR noted that at NATRE (Ledwell et al., 1993, 1998) the diapycnal mixing of heat, salt and tracer is dominated by turbulence but enhanced by salt fingers, and Kelley (2001) noted that at NATRE up to half of the diffusion (of an injected tracer) might have been transported by DD (St. Laurent and Schmitt, 1999; Kelley, 2001). Furthermore, from the maps of the oceanic sites susceptible to DD process presented in Figs. 6, 7 (kindly provided to us by Dr. D.E. Kelley), one observes that the likelihood of SF (salt fingers) processes is higher in the Atlantic (the location of NATRE) than in most of the Pacific and that DC (diffusive convection) may play a significant role in the Arctic and Southern oceans, a point discussed with extensive references by Kelley et al. (2003, Section 2.3.2) who concluded that DC "could be of major importance

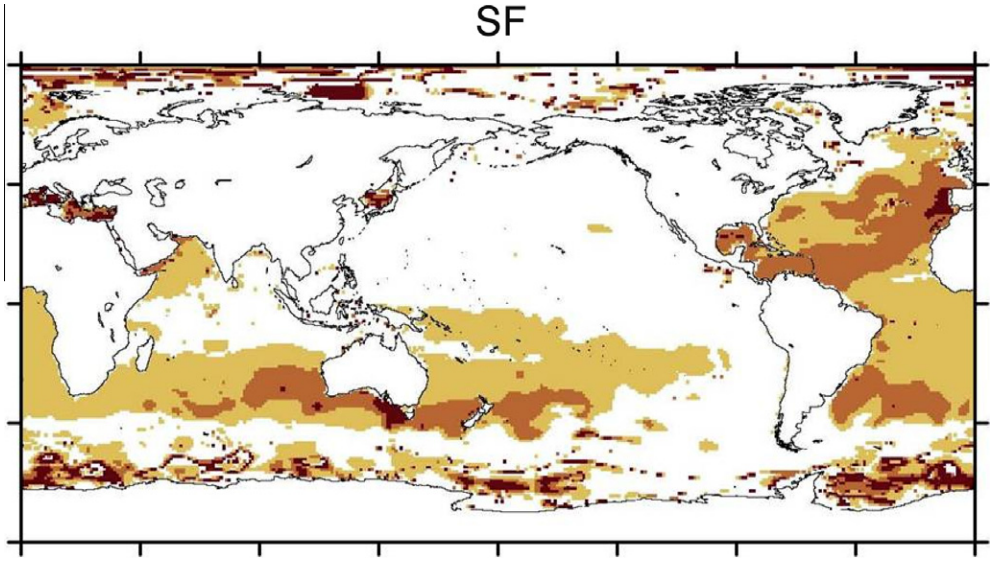

Fig. 6. Salt Fingers. Ocean regions susceptible to SF; R_ρ^{-1} intervals are: 1–1.5 (red), 1.5–2 (light brown) and 2–3 (yellow). The reddest color has the lowest R_ρ^{-1} which is most favorable to SF. Courtesy of D.E. Kelley.

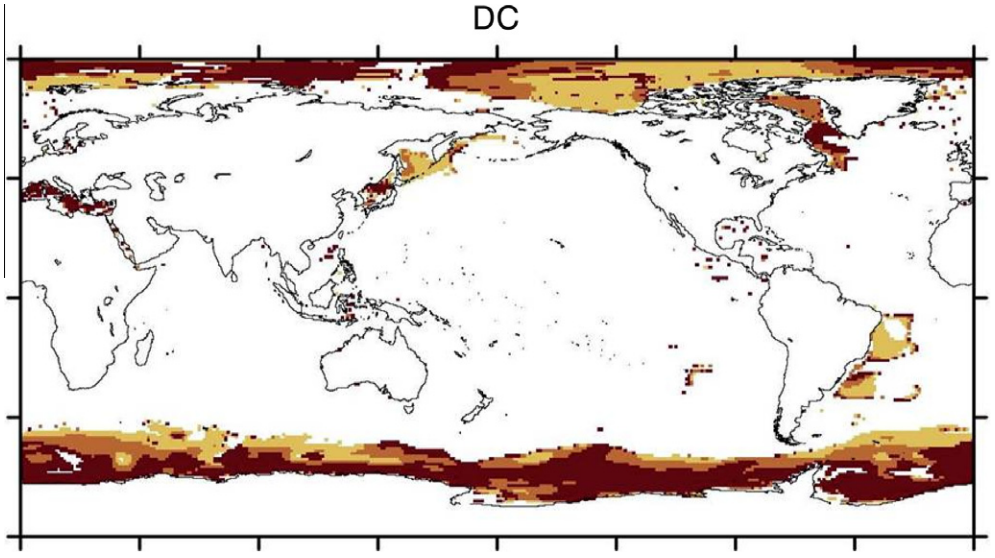

Fig. 7. Diffusive convection. Ocean regions susceptible to DC; R_ρ intervals are: 1–3 (red), 3–5 (light brown) and 5–10 (yellow). The reddest color has the lowest R_ρ which is most favorable to DC. Courtesy of D.E. Kelley.

to the properties of the global ocean". In general, DC is more likely in high-latitude precipitation zones (Schmitt, 1994) and Muench et al. (1990) also found it in Antarctica over much of the Weddell Sea. Overall, in the circumpolar current, both SF and DC may be quite important. In conclusion, the results of the present model are closer to the data than those of any previous models.

6. Modeling dissipation

As previously discussed, Eq. (20) for the dissipation ε has never been derived from first principles using two-point closures (see, however, Canuto et al. (2010)), it contains adjustable parameters whose sign is still in dispute, it does not contain double diffusion and it is not clear how to extend it to include internal gravity waves. Under such circumstances, the best one can do is to employ heuristic models, as we now discuss.

6.1. Mixed layer

We follow the methodology discussed in paper I, Section 11 and paper II, Section 9a and model ε as follows (Mellor and Yamada, 1982):

$$\varepsilon_{\rm ML} = \eta \ell^2 \Sigma^3, \quad \eta = \eta_0 (\tau \Sigma)^{-3} \tag{62}$$

Since the mixing length ℓ and the shear Σ are the natural variables, the combination $\ell^2\Sigma^3$ follows; the second relation in (62) comes from using the following relations $\varepsilon = K^{3/2}/\Lambda$, $\tau = 2K/\varepsilon$, $\Lambda = 8^{-1/2} B_1 \ell$, where the numerical coefficient $\eta_0 = B_1^2$ stems from the relation $\Lambda = 8^{-1/2} B_1 \ell$, where $B_1 = G_m^{3/4}(Ri = 0) = 21.6$ as discussed in Cheng et al. (2002). As for the mixing length, we employ the relation:

$$\ell_B^{-1} = (\kappa z)^{-1} + \ell_0^{-1} \tag{63}$$

which follows from Blackadar (1962) who suggested that the mixing length ℓ be taken as half of the harmonic mean of κz and $\ell_0 = 0.17$H, H being the depth of the mixed layer and $\kappa = 0.4$ the von Karman constant. The z-dependence in (63) is such that for small z's, one recovers the law of the wall $\ell \sim \kappa z$, whereas for larger z's, ℓ becomes a constant fraction of H, as indicated by LES (Moeng and Sullivan, 1994). Following previous authors, e.g., Large et al. (1997), H is where the potential density differs from the surface value by $|\sigma(H) - \sigma(0)| > 3 \times 10^{-5}$ g cm^{-3}. However, Zilitinkevich et al. (2007) found that to match boundary layer data the length scale had to be reduced for large values of the flux Richardson number. For the purposes of a model which includes salt and heat contributions to stratification, we use the flux Richardson number defined in (53). Since the ratio K_ρ/K_m depends on Ri, R_ρ, so does R_f. As Fig. 8a shows, at each R_ρ, as Ri increases towards infinity, R_f approaches a finite limit $R_{f\infty}$ which is still a function of R_ρ. Generalizing the formula of Zilitinkevich et al. (2007), we then write:

$$\ell = \ell_B \left(1 - \frac{R_f}{R_{f\infty}}\right)^{4/3} \tag{64}$$

The factor introduced by Zilitinkevich in the above length scale causes the mixed layer contribution to the diffusivity to fall off quickly below the mixed layer so that we may use it in the region below as well to allow a continuous transition. In the mixed layer, Ri is computed using the resolved large scale fields.

6.2. Thermocline

In this region, we have two main contributors, IGW (internal gravity waves) and double diffusion which we now discuss. We begin by generalizing relation (1b) in the following way:

$$K_\alpha = \Gamma_\alpha(Ri, R_\rho) \frac{\varepsilon_{\rm th}}{N^2} L(\theta, N) \tag{65a}$$

with:

$$L(\theta, N) = [f \,\mathrm{Arcosh}(N/f)][f_{30} \,\mathrm{Arcosh}(N_0/f_{30})]^{-1} \tag{65b}$$

where f_{30} means f computed at 30°, $N_0 = 5.24 \times 10^{-3}$ s^{-1} and $\varepsilon_{\rm th}$ is the dissipation in the thermocline. The function $L(\theta,N)$ accounts for the measured latitudinal dependence of the IGW spectra (Gregg et al., 2003) which affects all diffusivities. The effect of the latitude dependence on the sharpness of the tropical thermocline was studied in Canuto et al. (2004b). As for $\varepsilon_{\rm th}$, the best procedure would be to identify it with relation (58) which, formally, is quite general. This is, however, not a feasible procedure because we lack a model for the dissipation $\chi(Ri,R_\rho)$ of general validity while we have only a few values measured at selected locations, e.g., NATRE. Use of (58) everywhere would therefore be unjustified.

Next, consider the contribution of IGW to $\varepsilon_{\rm igw}$ which we quantify using the Gregg–Henyey–Polzin model (Polzin et al., 1995; Polzin, 1996; Kunze and Sanford, 1996; Gregg et al., 1996; Toole, 1998) which gives:

$$\frac{\varepsilon_{\rm igw}}{N^2} = 0.288A \ \ (\text{cgs units}) \tag{66}$$

where the dimensionless constant A accounts primarily for deviations from the Garrett–Munk background internal gravity wave spectrum and it varies at most by a factor of 2. If we employ again the NATRE data with $A = 1$, $N^2 = N^2_{\rm NATRE}$, we obtain from (66):

$$\varepsilon_{\rm igw} = 0.5 \ \ (10^{-9} \mathrm{W/kg}) \tag{67}$$

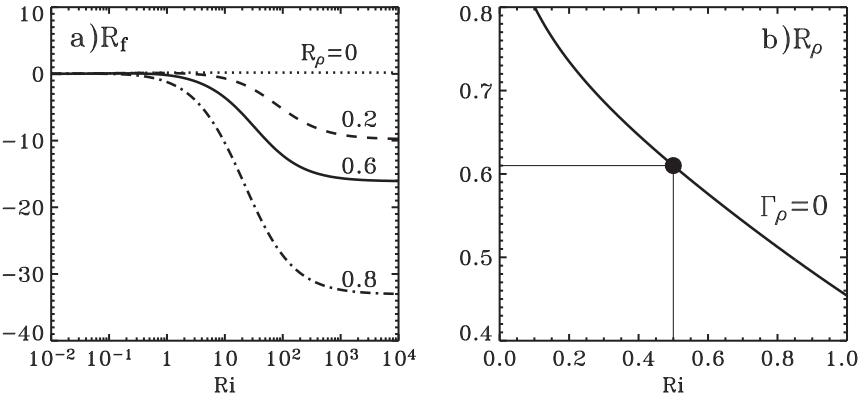

Fig. 8. (a) Same as in Fig. 3d with R_f re-plotted on a linear scale to exhibit negative values; (b) the values of R_ρ corresponding to $\Gamma_\rho = 0$ derived from Fig. 2d. The black dot indicates the value of $R_\rho = 0.61$ past which SF dominate over shear. The corresponding Ri is discussed in the text.

which is in the middle of Fig. 5a. For example, with an efficiency of $\Gamma_h = 0.25$, Eq. (66) yields a diffusivity of 0.07 $cm^2\ s^{-1}$ which is in accordance with the NATRE measurements (Ledwell et al., 1993). At present, lacking a more complete model, we shall use relations (65) with:

$$\frac{\varepsilon_{th}}{N^2} = 0.288 \ \text{(cgs units)} \tag{68}$$

The last problem concerns the *Ri* in (65). It cannot be identified with the large scale *Ri* for it would yield practically zero diffusivity. It must be a much lower value, which we call *Ri* (back), which is contributed mostly by the shear generated by the internal waves which is not resolved by the OGCMs and which must therefore be modeled. To identify *Ri* (back), we suggest the following procedure. Consider the plot Γ_ρ vs. *Ri* (Fig. 2d): we observe that Γ_ρ becomes negative at different *Ri* for different R_ρ. The physical meaning of the transition is as follows. While shear produces $\Gamma_\rho > 0$, DD produces $\Gamma_\rho < 0$: thus, we identify the change from $\Gamma_\rho > 0$ to$\Gamma_\rho < 0$ as the transition to a DD regime. In addition, since Schmitt and Evans (1978) and Zhang and Huang (1998) showed that SF become prevalent only at/or past $R_\rho \approx 0.6$, this value is plotted in Fig. 8b ($Ri - R_\rho$ points corresponding to $\Gamma_\rho = 0$) as a horizontal line. The corresponding $Ri \approx 0.5$ is taken to be the value of *Ri* (back).

It must be stressed that we are *not* suggesting that the measured values of *Ri* below the mixed layer be identified with *Ri* (back). Instead, we view *Ri* (back) as an effective *Ri* at which the diffusivity approximates the average of the diffusivities over a region of space and time containing points with a wide range of *Ri*. We take the point of view that the heat and salt diffusivities produced by SF, IGW shear mixing, and the interaction of the two, have spatial and temporal scales larger than those of the two processes separately. In building models for coarse OGCMs that do not resolve IGW or patches of SF, we can only attempt to model these large scale diffusivities. While the offline results in Fig. 4 show that our mixing model can reproduce the results of local measurements, they also illustrate the difficulty of translating such success into an OGCM parameterization. In fact, even after restricting to a SF favorable R_ρ and removing 75% of the data with lower dissipation, SS99 data in Fig. 4 still show a wide range of *Ri*, that is, for a fixedR_ρ, the measured *Ri* may vary from less than 0.25 to greater than 5. A single OGCM point represents a range of conditions including those where wave breaking produces strong shears and small *Ri*, as well as quiescent regions where no wave-breaking is occurring and *Ri* is large. With *Ri* (back), we attempt to represent the effects of this whole range of *Ri*'s that the OGCM does not resolve. Although most of the data points in Fig. 4 for $R_\rho = 0.6$ have $Ri > 0.5$, it must be remembered that the lowest *Ri* entails large diffusivities and thus carry greatest weight in the average diffusivity.

However, there remains the question of the dependence of *Ri* (back) on R_ρ. In paper II, *Ri* (back) was taken to be a fraction of *Ri*(cr), the latter being traditionally defined as the value past which turbulent mixing vanishes. On the other hand, since in the present more realistic model there is no longer an *Ri*(cr), the approach in II is no longer viable. We have examined several alternatives to find the R_ρ dependence of *Ri* (back) but have not yet obtained a credible result. While the search continues, we decided to examine the simplest case of taking *Ri* (back) constant. Since *Ri* (back) is introduced to produce average diffusivities for coarse resolution OGCMs, it must be tested against averaged data. In Fig. 9, we compare the mass diffusivity K_ρ from the model with *Ri* (back) = 0.5 with the SS99 data which are averages over many measurements (the 90 meter point was excluded because there may be contamination from the boundary layer and the error bar on the measurement is quite large).

Since the model vs. data are in reasonable agreement, we feel that while we keep on searching to improve it, the relation *Ri* (back) = 0.5 is a tolerable, provisional approximation.

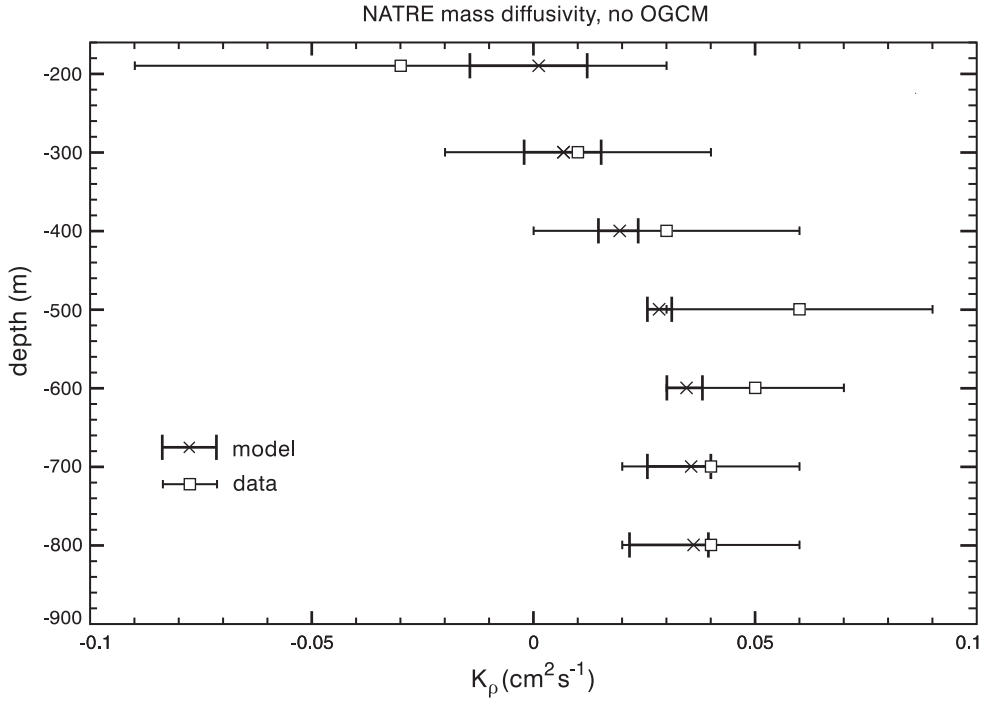

Fig. 9. NATRE: the crosses represent the mass diffusivity K_ρ defined in Eq. (55) as a function of depth at the location of NATRE without use of an OGCM. The heat and salt diffusivities in Eqs. (55) and (32) are given by the model as a functions of both *Ri* and R_ρ, together with Eq. (68). The values of R_ρ are taken from the St. Laurent and Schmitt (1999) data while *Ri* is taken to be 0.5, as discussed in the text. The error bars of the model results reflect the errors bars in R_ρ. The squares represent the SS99 data with error bars.

7. Tides

The effect of tides was studied by several authors (Kantha et al., 1995; Munk, 1966, 1997; Munk and Wunsch, 1998; St. Laurent et al., 2002; St. Laurent and Garrett, 2002; Garrett and Kunze, 2007; Munk and Bills, 2007) and it requires the modeling of three distinct processes: (a) *enhanced bottom diffusivity* due to baroclinic tides, (b) *tidally induced drag*, and (c) *unresolved bottom shear*, which we now discuss in that order.

7.1. Internal, baroclinic tides

To generate bottom mixing, the key physical process has been identified to be the conversion of barotropic into baroclinic tides caused by the interaction of the former with rough bottom topography. The non-linear interactions among the baroclinic tides (and the shear they contain) allow part of their energy to be used to raise the center of gravity and thus produce mixing.

The conversion of barotropic tides into baroclinic internal tides was studied by several authors, e.g., Kantha and Tierney (1997), Llewellyn Smith and Young (2002), St. Laurent and Garrett (2002) and Legg (2004) and was included in OGCMs by two groups (Simmons et al., 2004, cited as S4; Saenko and Merryfield, 2005, cited as S5). Here, we employ the work of one of the present authors (S.R. Jayne). One begins by solving offline the 2D Laplace tidal equation with a resolution of 1/2° to obtain the barotropic tidal velocity $\mathbf{u}_t$, the 2D dynamical equations contain a drag which depends on the bottom topographic roughness denoted by h which is taken from the Smith and Sandwell (1997) data at 1/32° resolution and then binned into the 1/2° resolution of the 2D code that provides $\mathbf{u}_t$. With the latter, one then constructs an expression for the internal tidal energy $E(x,y)$ using the following parameterization by Jayne (2009):

$$E(x,y) = \frac{1}{2}\bar{\rho} N \kappa h^2 \overline{\mathbf{u}_t^2} \ (\mathrm{W\,m^{-2}}) \tag{69}$$

where (κ,h) are the wavenumber and amplitude. As discussed in Jayne (2009), the topographic roughness h^2 was derived from high resolution bathymetry [US Department of Commerce, 2006: 2-min Gridded Global Relief Data (ETOPO2v2). National Oceanic and Atmospheric Administration, National Geophysical Data Center. Available online at http://www.ngdc.noaa.gov/mgg/fliers/06mgg01.html; Smith and Sandwell, 1997] as the root-mean-square of the topography over a 50-km smoothing radius, and κ is a free parameter set as $\kappa = 2\pi/125$ km. It should be emphasized that Eq. (69) is a scale relation and not a precise specification of internal tide energy flux. In the barotropic tidal model, the value of $\kappa = 2\pi/125$ km was tuned to give the best fit to the observed tides. To construct the required $\varepsilon_{\mathrm{tides}}$, we employ the model suggested by St. Laurent et al. (2002) which has the following form:

$$\begin{aligned} &\rho\varepsilon_{\mathrm{tides}} = qE(x,y)F(z) \\ &F(z) = A\zeta^{-1}\exp[-(H+z)/\zeta], \quad A^{-1} \equiv 1 - \exp[-(H/\zeta)] \end{aligned} \tag{70}$$

where the role of z^{-1} is played by the scale function $F(z)$ in which $\zeta = 500$ m. The parameter q accounts for the fact that only a fraction q of the baroclinic energy goes into creating mixing; the remaining part $1-q$ is radiated into the ocean interior where it may contribute to the background diffusivity. The last step is the construction of the tidally-induced diffusivity using relation (1b):

$$K_\alpha = \Gamma_\alpha(Ri, R_\rho)\frac{\varepsilon_{\mathrm{tides}}}{N^2} \tag{71}$$

Since S4,5 also used (69)–(71), we need to point out the differences with their analysis. *First*, S4,5 used $\Gamma = 0.2$ for heat and salt while for momentum S4 took $K_m = 10K_{h,s}$ and S5 took $K_m = 10^{-4}\mathrm{m^2\,s^{-1}}$, whereas in our model we have different heat, salt and momentum mixing efficiencies that depend on Ri and R_ρ. This means that since these efficiencies are different, the mean T, S and velocity will be affected differently by tides. *Second*, we have updated the Jayne and St. Laurent's (2001) original method. In particular, the model domain was expanded to cover the global ocean (rather than ±72° as in the original work). Additionally, the gravitational self-attraction and loading in the tidal model was implemented in an iterative manner as in Arbic et al. (2004). Overall, these changes improve the fit of the simulated tides slightly: the diurnal tides improved significantly, likely due to including all of the Southern Ocean, where the diurnal tides are large, and the simulated semidiurnal tides did not improve. Though other parameterizations of the internal wave conversion were suggested by Arbic et al. (2004) and Egbert et al. (2004), it was found that all of the schemes gave comparable accuracies in the simulated tidal elevations. The new expression for $E(x,y)$ is taken from Jayne (2009). Third, in the case of tides the Ri in (71) was taken to be the background value 0.5.

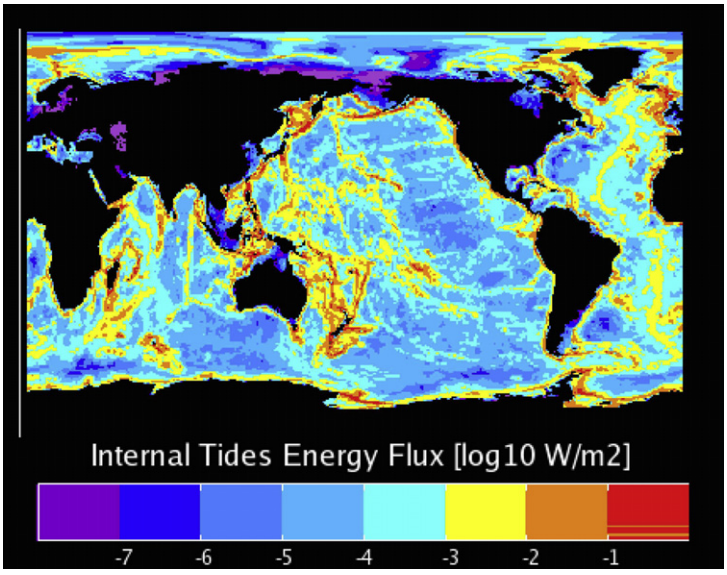

Fig. 10a. Base 10 logarithm of the internal tidal energy flux E, Eq. (69), in units of $\mathrm{W\,m^{-2}}$.

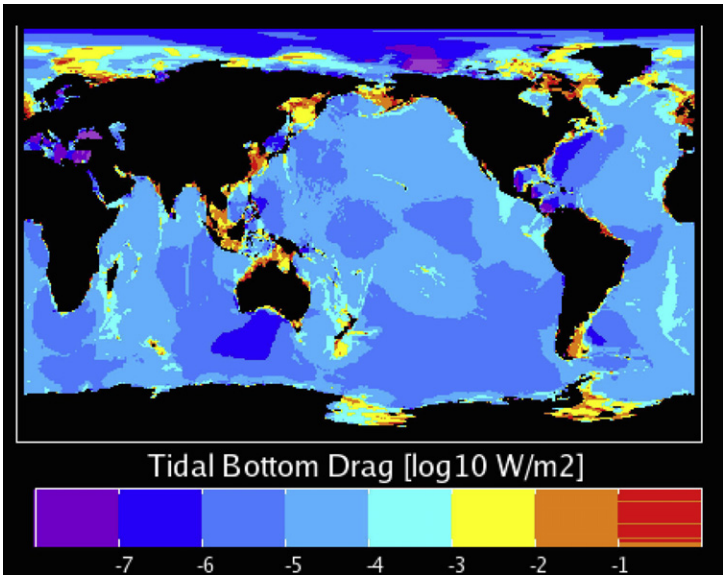

Fig. 10b. Drag power in W m^{-2} from the tidal velocities u_t from Jayne and St. Laurent (2001). In Figs. 10a and 10b, the model is extended past ±72° that characterized the analogous figures in Jayne and St. Laurent (2001).

7.2. Tidal drag, shallow seas

Since the tidal energy of 1.51 Terawatts (Egbert and Ray, 2000, 2003) dissipated as tidal drag is only 30% smaller than the one in internal tides, it is necessary to account for it. As is the case in Fig. 10a, the drag power in W m^{-2} shown in Fig. 10b corresponds to the updated model while the analogous figure in Jayne and St. Laurent (2001) corresponded to the old model ±72°. Contrary to internal tides, tidal drag cannot be represented by a diffusivity and its modeling is a non-trivial problem for several reasons. The bottom tidal velocity is generally larger than the mean velocity, for example, in shallow seas the tidal velocities are $O(5)$ cm s^{-1} which are much larger than $O(0.5)$ cm s^{-1} characterizing the mean velocities (Webb and Suginohara, 2001a,b; Garrett and St. Laurent, 2002).

We begin by considering the component of the tidal field's velocity that is along the direction of the mean field which can be modeled as an increased mean drag. That is done by extending the traditional quadratic bottom drag formula that depends only on the resolved mean flow $\bar{\mathbf{u}}$ to include the tidal velocities $\mathbf{u}_t$ so that the total velocity field is now $\mathbf{u} = \bar{\mathbf{u}} + \mathbf{u}_t$. Beckmann (1998) and Haidvogel and Beckmann (1999, Eq. (5.19)) suggested the following expression:

$$\boldsymbol{\tau}_b = C_D \mathbf{u}|\mathbf{u}| \to C_D \bar{\mathbf{u}} \left(\bar{\mathbf{u}}^2 + \overline{\mathbf{u}_t^2}\right)^{1/2}, \quad C_D = 0.003 \tag{72}$$

but since we did not find a derivation of it, we present one in Appendix C. The tidal velocities were taken from the same tidal model used to compute the function $E(x,y)$ in Eq. (69) and therefore the tidal contribution is location dependent.

Two OGCMs have employed (72), the OCCAM Code 66 level model (SOC Inter. Report No. 99; http://www.noc.soton.ac.uk/jrd/occam, 2005) and the GFDL Code (Griffies, private communication, 2008). However, in both cases, the tidal velocity was taken to be constant while we employ the one derived from a tidal model and thus location and topography dependent.

7.3. Unresolved bottom shear

The component of the tidal field not aligned with the mean velocity cannot be modeled as a tidal drag. Since its mean shear is not zero and often large, it gives rise to a large unresolved shear $\Sigma_{\rm unr}$ with respect to the ocean's bottom. This additional shear decreases the local Ri possibly bringing it below $Ri = O(1)$, thus allowing shear instabilities to occur which ultimately enhance the diffusivities.

We know of only one work (Lee et al., 2006) that includes $\Sigma_{\rm unr}$ in an OGCM using a heuristic expression for $\Sigma_{\rm unr}$ that depends on the M2 tidal velocity obtained from satellite data (Egbert et al., 1994). Rather than using a heuristic expression for $\Sigma_{\rm unr}$, we adopted the viewpoint that since modeling an unresolved shear is a problem that has been widely studied in the context of the PBL (planetary boundary layer), there is a well assessed formalism we can adopt and which results in the following expression (Businger et al., 1971; Kaimal and Finnigan, 1994; Cheng et al., 2002):

$$\Sigma_{\rm unr} = \frac{u_*}{\kappa z} \Phi_m \tag{73}$$

where u^* is a frictional velocity and $\Phi_m(z/L)$ is a dimensionless structure function of the dimensionless ratio z/L where L is the Monin–Obukov length scale. Several field tested expressions for $\Phi(Ri)$ are available in the literature (e.g., Kaimal and Finnigan, 1994). However, since Cheng et al. (2002) derived an expression for $\Phi(Ri)$ from the RSM which is the formalism used in this work, for consistency reasons, we have adopted Cheng et al.'s expression for $\Phi(Ri)$ which was shown to reproduce previous empirical forms assessed against field experiments, the classical one being the Kansas experiment discussed in detail by Businger et al. (1971). As for u^*, we model it in terms of the mean and tidal velocities. To do so, we consider the first relation (72) with $\mathbf{u} = \bar{\mathbf{u}} + \mathbf{u}_t$:

$$\begin{aligned}\boldsymbol{\tau}_b(\text{total}) &= C_D \bar{\mathbf{u}} \left(\bar{\mathbf{u}}^2 + 2\bar{\mathbf{u}} \cdot \mathbf{u}_t + \mathbf{u}_t^2\right)^{1/2} \\ &\quad + C_D \mathbf{u}_t \left(\bar{\mathbf{u}}^2 + 2\bar{\mathbf{u}} \cdot \mathbf{u}_t + \mathbf{u}_t^2\right)^{1/2}\end{aligned} \tag{74}$$

In order to exhibit the contribution of the unresolved scales, we subtract from (74) its average thus yielding the unresolved part which then gives the desired u^*:

$$\boldsymbol{\tau}_b(\text{unr}) = \boldsymbol{\tau}_b(\text{total}) - \overline{\boldsymbol{\tau}_b(\text{total})} \qquad u_*^2 \equiv \left[\overline{\boldsymbol{\tau}_b^2(\text{unr})}\right]^{1/2} \tag{75}$$

In Appendix C we derive the following expression:

$$\left[\overline{\tau_b^2(\mathrm{unr})}\right]^{1/2} = C_D\left(\overline{\mathbf{u}_t^2}\right)^{1/2}\left(\bar{\mathbf{u}}^2 + \overline{\mathbf{u}_t^2}\right)^{1/2} \tag{76}$$

The $\overline{\mathbf{u}_t^2}$ from the tidal model averaged to the resolved scales characterizing the OGCM one employs, is used in (76) and the results are substituted into (75) and finally (73) to construct the Richardson number in which the shear is now given by:

$$Ri = \frac{N^2}{\Sigma^2}, \quad \Sigma^2 = \Sigma^2_{\mathrm{res}} + \Sigma^2_{\mathrm{unr}} \tag{77}$$

where Σ^2_{res} is the square of the shear of the resolved velocity field.

8. Diapycnal velocity

Once an OGCM is run using the mixing scheme just presented, the resulting large scale fields can be used to evaluate the diapycnal velocity w^* which is an important part of the discussion on the origin of the MOC (meridional overturning circulation, Munk, 1966, 1997; Munk and Wunsch, 1998, cited as MW; Döös and Webb, 1994; Döös and Coward, 1997; Toggweiler and Samuels, 1998; Webb and Suginohara, 2001a,b).

Since our mixing scheme includes DD processes and since we were unable to find an expression of w^* that includes different heat and salt diffusivities, we present such formula with some comparison with previous expression and some qualitative implications. Multiplying the mean temperature and salinity equations by $\alpha_{T,S}$, respectively, and subtracting the two equations, one obtains the following expression for the diapycnal diffusivity w^*:

$$\begin{aligned} N^2 w^* &= g\left[\alpha_T \frac{\partial}{\partial z}\left(K_h \frac{\partial T}{\partial z}\right) - \alpha_S \frac{\partial}{\partial z}\left(K_S \frac{\partial S}{\partial z}\right)\right] \\ &= \frac{\partial}{\partial z}(K_\rho N^2) - N^2(1-R_\rho)^{-1} K_h\left(\frac{\alpha_{T,z}}{\alpha_T} - r^{-1}\frac{\alpha_{s,z}}{\alpha_s}\right) \end{aligned} \tag{78}$$

where $a_{,z} = \partial a/\partial z$ and where the spatial variation of the coefficients $\alpha_{T,S}$ is due to the non-linearity of the seawater equation of state. In (78) we have not included cabbeling and thermobaricity which can be added, as shown in Klocker and McDougall (2010, in press). From the second form in (78), it is easy to check that if one takes:

$$\alpha_{T,S} : z\text{-independent} \tag{79}$$

Eq. (78) reduces to the first term only which is the form of the advective–diffusive balance used by MW:

$$w^* = N^{-2}\frac{\partial}{\partial z}(K_\rho N^2) \tag{80}$$

Since MW further considered only positive $K_\rho > 0$, it means that they did not include DD processes: thus, the MM model for w^* does not include non-linearities in the seawater EOS nor does it include DD. On the other hand, if one consider the case:

$$\begin{aligned} &\text{No DD}: \ K_h = K_s = K_\rho \to D \\ &\text{Non-linearities in the seawater EOS}: \ \alpha_{T,S} : z\text{-dependent} \end{aligned} \tag{81}$$

Eq. (78) reduces to

$$N^2 w^* = \frac{\partial}{\partial z}(\mathrm{DN}^2) - \mathrm{DN}_h^2\left(\frac{\alpha_{T,z}}{\alpha_T} - r^{-1}\frac{\alpha_{s,z}}{\alpha_s}\right) \tag{82}$$

which is Eq. (23) of Klocker and McDougall (2010, in press).

Even without numerical computations, one can use the previous relations to derive some interesting results concerning the effects of DD and tides. Clearly, what follows has an illustrative value only. We first employ a constant diffusivity and a profile of N^2 of the type $N^2(z) = N_0^2 e^{(z-H)/h}$ (Zang and Wunch, 2001), which gives, using relation (80):

$$w^* = h^{-1}K_\rho \qquad Q(Sv) = Aw^* = Ah^{-1}K_\rho \tag{83}$$

where A is the surface of the ocean, $z = 0$ corresponds to the ocean's bottom and $z = H$ is the surface value and $N^{-2}\partial N^2/\partial z = h^{-1}$. In the MW paper, the integral of $N^2(z)$ between 1 and 4 km was taken to be $g\Delta\rho/\rho = g10^{-3}$; in our notation this corresponds to $h = 1.3$ km and thus we obtain:

$$K_\rho = 1\ \mathrm{cm^2\ s^{-1}} : Q = 28\ \mathrm{Sv}, \quad K_\rho = 0.1\ \mathrm{cm^2\ s^{-1}} : Q = 2.8\ \mathrm{Sv} \tag{84}$$

the first of which coincides with the case studied by MW. Next, we consider the contribution of tides. Using Eq. (70), the previous model for N^2, and the MW model, we obtain:

$$w^* = N^{-2}\frac{\partial K_\rho N^2}{\partial z} = K_\rho\left(\frac{1}{h} - \frac{1}{\zeta}\right) \tag{85}$$

Depending on the relative sizes of the two scale heights, h, ζ, there may be an upwelling or a downwelling. For example, using $\zeta = 500$ m, as discussed previously, Eq. (85) implies that *tides cause downwelling*:

$$Q(\mathrm{tides}) < 0 \tag{86}$$

Next, we consider the effect of Double Diffusion. Using Eqs. (1b) and (27), the $P = \varepsilon$ relation given by Eq. (26) becomes:

$$Ri^{-1}\Gamma_m - \Gamma_\rho = 1 \tag{87}$$

Since a necessary condition for DD processes to exist is the absence of strong shear, we take $Ri \gg 1$ and thus $\Gamma_\rho = -1$ which means that the diffusivity becomes:

$$K_\rho = \Gamma_\rho\frac{\varepsilon}{N^2} = -\frac{\varepsilon}{N^2} \tag{88}$$

and thus:

$$w^* = N^{-2}\frac{\partial \varepsilon\Gamma_\rho}{\partial z} = -N^{-2}\frac{\partial \varepsilon}{\partial z} \tag{89}$$

Depending on whether, in the DD dominated regime, $\varepsilon(z)$ increases or decreases with depth, we may have either upwelling or downwelling due to DD processes. The data in Figs. 13–16 of Kunze et al. (2006) do not allow us to draw a firm conclusion.

9. Conclusions

The complete mixing model which is composed of the RSM results and different models for the dissipation ε, is summarized in Appendix B. In the local limit, which is a justifiable approximation in a stably stratified regime, the RSM is fully algebraic and it only requires the solution of the cubic Eq. (41). The reason why it is presented in a nested form is twofold: the physics of the various terms is easier to follow and from the numerical-computational viewpoint, nested relations are more advantageous. The physical aspect of the RSM is exhibited in relations (1) which show the key role played by the mixing efficiencies Γ_α or by the structure functions S_α which depend on Ri, R_ρ and on the dynamical time scale which, in units of the mean shear, forms the dimensionless combination $(\tau\Sigma)^2$ whose dependence on Ri, R_ρ is obtained by solving the cubic equation (41) which yields (28). These functions S_α and Γ_α are different for heat, salt and momentum, as shown in Figs. 1 and 2. We have assessed the validity of the RSM results based on production = dissipation by comparing predictions vs. measured data. The tests without an OGCM are as follows.

Turbulent Prandtl number vs. Ri, Fig. 3c. There are abundant data that yield the ratio of the momentum to heat diffusivity vs. *Ri*

though only in the absence of DD processes. The data are reproduced satisfactorily.

Flux Richardson number, R_f vs. Ri, Fig. 3d. The RSM predictions reproduce the data without DD satisfactorily.

DD processes. Past work by several authors showed how difficult it has been to construct a mixing model with DD + background turbulence. Our predictions provide a reasonable fit to the oceanic data, specifically:

Mixing efficiency $\Gamma_h(Ri,R_\rho)$, Fig. 4. The data exhibit a clear dependence on Ri and R_ρ and, as discussed in Section 5.8, previous models based on linear analysis and laboratory data were not successful in constructing a DD model in a mildly turbulent background. Laboratory data correspond to regimes with no shear that is, $Ri \to \infty$, and their use in an ocean context is of doubtful validity.

Bimodal ε*-distribution*, Fig. 5a. The finding by SS99 of a bimodal kinetic energy dissipation ε, namely that in the SF regime $Ri > 1$, ε is an order of magnitude smaller than in the case of turbulence $Ri < 1$, is reproduced rather closely.

Heat to salt flux ratio $r(Ri,R_\rho)$, Fig. 5b. In the regime of vanishing shear, the RSM predictions of the heat to salt flux ratio reproduce satisfactorily the data presented in Fig. 10a of SS99.

NATRE mass diffusivity, Fig. 9 (St. Laurent and Schmitt, 1999). The model error range (obtained using data ranges for R_ρ), in most cases lies inside the data error range and in all cases intersects it.

Tides. To describe the effect of tides, one must account for three distinct features: internal tides, tidal drag and the unresolved bottom shear. Internal tides were modeled in the same way as previous authors via Eqs. (69)–(71) but the mixing efficiencies were not taken to be the same for heat, salt and momentum, rather, they were computed from within the model using relations (5) and the function $E(x,y)$ was taken from an updated model by one of the authors (Jayne, 2009). Tidal drag, which is most relevant in shallow seas, was only approximately accounted for in previous studies whereas we employ the results of the tidal model to compute the bottom drag rather than assuming a constant tidal velocity, as done previously. As for the unresolved bottom shear, we have now included the tidal velocities not aligned with the mean velocities since they increase the shear, decrease Ri and enhance mixing. To model the unresolved shear, we adopted a procedure that has been successfully used in PBL studies.

To assess the effect of the physical processes described above on the ocean's global properties, one needs to employ an OGCM with a relatively high vertical resolution. For example, tidal drag which is expected to be the strongest in shallow seas, cannot be well represented in OGCMs in which some shallow regions are converted to land or deepened due to the coarse horizontal gridding and requirements of numerical stability. Moreover, the OGCM treatment of deep regions using very thick layers near the bottom may not be able to resolve the bottom boundary layer so that the new effects, which are highly localized to the bottom, as opposed to the tidal energy which radiates upward with scale height $\sim$1/2 km, may not be allowed to act in full. Furthermore, the fact that often OGCM assign only one depth to each gridcell, whereas in regions of rough topography the true depth of the ocean bottom varies greatly over a gridcell's area, degrades the performance of the tidal model. OGCMs with both high horizontal resolution and finer spacing in the vertical near the bottom and/or a parameterization which accounts for the actual distribution of bottom depths within each gridcell, are needed to fully assess the new mixing scheme.

Future studies should also include into the mixing scheme the effect of mesoscales (30–100 km) and sub-mesoscales O(1 km). It is well documented that they both re-stratify the mixed layer thus producing a reduction in the mixed layer depth (Oschlies, 2002; Mahadevan et al., 2010). No OGCM that we know of has included such mixed layer effects since there is still no satisfactory parameterization of such processes. In addition, suggestions have been made that even in the deep ocean mesoscales may not move strictly along isopycnal surfaces, as assumed thus far: if they do not, there is a further contribution to the diapycnal diffusivity in addition to the small scale one discussed here. Recent studies (Tandon and Garrett, 1996; Eden and Greatbatch, 2008a,b) have concluded that the effect may not be negligible especially at the ocean bottom.

Note added in proofs

It has been pointed out to us that in a recent paper, T. Decloedt and D.S. Luther (2010) have suggested a polynomial alternative to the exponential scale function F(z) in Eq. (70), which, as seen in their Fig. 4, provides a better fit to the data. Such a new formula, their Eq. (2), can easily be adopted in this model instead of the function F(z) in Eq. (70). We want to thank Dr. J. Richman for pointing out this reference to us.

Acknowledgements

V.M.C. expresses his thanks to three anonymous referees and to Dr. S. Griffies for suggestions and criticism that were instrumental in improving the manuscript through several revisions. A.M.H. thanks Dr. D.J. Webb for correspondence regarding the OCCAM code and Dr. J. Marotzke for correspondence regarding the MOC and heat transport. V.M.C., A.M.H. and C.J.M. thank Mr. Leonardo Caputi, a summer student who helped us in many important ways to prepare the results presented in the figures.

Appendix A. 1D form of the Reynolds stress equations

Vertical heat flux, $J^h = \overline{w\theta}$:

$$\frac{DJ^h}{Dt} = -\overline{w^2}T_{,z} + g\left(\alpha_T\overline{\theta^2} - \alpha_s\overline{\theta s}\right) - \tau^{-1}\pi_4^{-1}J^h \tag{A.1}$$

Vertical salt flux, $J^s = \overline{ws}$:

$$\frac{DJ^s}{Dt} = -\overline{w^2}S_{,z} + g\left(\alpha_T\overline{\theta s} - \alpha_s\overline{s^2}\right) - \tau^{-1}\pi_1^{-1}J^s \tag{A.2}$$

Temperature variance, $\overline{\theta^2}$:

$$\frac{D\overline{\theta^2}}{Dt} = -2J^hT_{,z} - 2\tau^{-1}\pi_5^{-1}\overline{\theta^2} \tag{A.3}$$

Salinity variance, $\overline{s^2}$:

$$\frac{D\overline{s^2}}{Dt} = -2J^sS_{,z} - 2\tau^{-1}\pi_3^{-1}\overline{s^2} \tag{A.4}$$

Temperature-salinity correlation, $\overline{\theta s}$:

$$\frac{D\overline{\theta s}}{Dt} = -J^hS_{,z} - J^sT_{,z} - \tau^{-1}\pi_2^{-1}\overline{\theta s} \tag{A.5}$$

Traceless Reynolds stress tensor $b_{ij} = \tau_{ij} - 2\delta_{ij}K/3$ $(i,j = 1,2,3)$:

$$\frac{Db_{ij}}{Dt} = -\frac{8K}{15}S_{ij} - \frac{1}{2}Z_{ij} + \frac{1}{2}B_{ij} - \frac{5}{\tau}b_{ij} \tag{A.6}$$

with:

$$Z_{ij} = b_{ik}V_{jk} + b_{jk}V_{ik}, \quad B_{ij} = g\left(\lambda_iJ_j^\rho + \lambda_jJ_i^\rho - \frac{2}{3}\delta_{ij}\lambda_kJ_k^\rho\right) \tag{A.7}$$

where $S_{ij} = 1/2(U_{i,j} + U_{j,i})$ and $V_{ij} = 1/2(U_{i,j} - U_{j,i})$ are the (mean) shear and vorticity tensors and J_i^ρ is defined as follows:

$$J_i^\rho = \alpha_TJ_i^h - \alpha_sJ_i^s, \quad \lambda_i \equiv -(g\bar{\rho})^{-1}\overline{p}_{,i} \tag{A.8}$$

Since Eqs. (A.6) involve also the horizontal heat and salinity fluxes via the buoyancy tensor B_{ij}, one needs to account for their presence. The corresponding equations are:

Horizontal heat flux, $J_i^h = \overline{u_i\theta},\ i = 1,2$:

$$\frac{DJ_i^h}{Dt} = -\overline{u_i w}T_{,z} - J^h\partial_z U_i - \tau^{-1}\pi_4^{-1}J_i^h \tag{A.9}$$

Horizontal salt flux, $J_i^s = \overline{u_i s},\ i = 1,2$:

$$\frac{DJ_i^s}{Dt} = -\overline{u_i w}S_{,z} - J^s\partial_z U_i - \tau^{-1}\pi_1^{-1}J_i^s \tag{A.10}$$

Dissipation-relaxation time scales:

For $R_\rho > 0$ and $Ri > 0$,

$$\begin{aligned}
&\pi_1 = \pi_1^0\left(1+\frac{RiR_\rho}{a+R_\rho}\right)^{-1}, \quad \pi_4 = \pi_4^0\left(1+\frac{Ri}{1+aR_\rho}\right)^{-1},\\
&\pi_2 = \pi_2^0(1+Ri)^{-1}\left[1+2RiR_\rho(1+R_\rho^2)^{-1}\right], \quad \pi_5 = \pi_5^0,\\
&\pi_1^0 = \pi_4^0 = (27Ko^3/5)^{-1/2}(1+\sigma_t^{-1})^{-1},\\
&\pi_2^0 = 1/3, \quad \pi_3 = \pi_3^0 = \pi_5^0 = \sigma_t,
\end{aligned} \tag{A.11}$$

where $a = 10$, $Ko = 1.66$ and σ_t was taken from Eq. (10b). For $R_\rho \leqslant 0$ and $Ri > 0$, we further have the relations:

$$\pi_{1,4} = \pi_{1,4}^0(1+Ri)^{-1}, \quad \pi_{2,3,5} = \pi_{2,3,5}^0 \tag{A.12}$$

On the other hand, for $Ri \leqslant 0$, $\pi_k = \pi_k^0$ for any k.

Appendix B. Complete mixing model

Here, we summarize the complete form of the mixing model.

Diffusivities (α = heat, salt, momentum, density)

$$\text{General form}: \quad K_\alpha = S_\alpha\frac{2K^2}{\varepsilon} = \Gamma_\alpha\frac{\varepsilon}{N^2}, \quad \Gamma_\alpha \equiv \frac{1}{2}Ri(\tau\Sigma)^2S_\alpha \tag{B.1}$$

$$\text{Structure functions}: \quad S_\alpha = A_\alpha\frac{\overline{w^2}}{K} \tag{B.2}$$

Heat and salt:

$$A_h = \pi_4\left[1+px+\pi_4\pi_2x(1-r^{-1})\right]^{-1}, \quad A_s = A_h(rR_\rho)^{-1} \tag{B.3}$$

Heat-to-salt flux ratio:

$$r \equiv \frac{\alpha_T\overline{w\theta}}{\alpha_s\overline{ws}} = \frac{\pi_4}{\pi_1}\frac{1}{R_\rho}\frac{1+qx}{1+px} \tag{B.4}$$

Momentum:

$$S_m = A_m\frac{\overline{w^2}}{K}, \quad A_m = \frac{A_{m1}}{A_{m2}} \tag{B.5}$$

where:

$$A_{m1} = \frac{4}{5} - \left[\pi_4 - \pi_1 + \left(\pi_1 - \frac{1}{150}\right)(1-r^{-1})\right]xA_h \tag{B.6}$$

$$A_{m2} = 10 + (\pi_4 - \pi_1R_\rho)x + \frac{1}{50}(\tau\Sigma)^2 \tag{B.7}$$

Ratio $\frac{\overline{w^2}}{K}$:

$$\frac{\overline{w^2}}{K} = \frac{2}{3}\left[1+\frac{2}{15}X+\frac{1}{10}A_m(\tau\Sigma)^2\right]^{-1}, \quad X \equiv (1-r^{-1})xA_h \tag{B.8}$$

Dimensionless variables x, p and q:

$$\begin{aligned}
&x = Ri(\tau\Sigma)^2(1-R_\rho)^{-1}, \quad p = \pi_4\pi_5 - \pi_4\pi_2(1+R_\rho),\\
&q = \pi_1\pi_2(1+R_\rho) - \pi_1\pi_3R_\rho
\end{aligned} \tag{B.9}$$

Dynamical time scale $G_m \equiv (\tau\Sigma)^2$ in the $P = \varepsilon$ model:

Cubic equation valid throughout the water column:

$$c_3G_m^3 + c_2G_m^2 + c_1G_m + 1 = 0 \tag{B.10}$$

with:

$$c_3 = A_1Ri^3 + A_2Ri^2, \quad c_2 = A_3Ri^2 + A_4Ri, \quad c_1 = A_5Ri + A_6 \tag{B.11}$$

where:

$$\begin{aligned}
150(1-R_\rho)^3A_1 &= \pi_1\pi_4(\pi_4 - \pi_1R_\rho)\left\{\pi_2(15\pi_3+7)\left(R_\rho^2+1\right)\right.\\
&\quad\left.+\left[14(\pi_2-\pi_3) - 15\pi_3^2\right]R_\rho\right\}
\end{aligned}$$

$$\begin{aligned}
9000(1-R_\rho)^2A_2 &= \pi_1\pi_4\left\{\pi_2(210\pi_1 - 150\pi_3 + 7)\left(R_\rho^2+1\right)\right.\\
&\quad+\left[14(\pi_2-\pi_3)(1+15\pi_1+15\pi_4) + 150\pi_3^2\right]R_\rho\\
&\quad\left.+210\pi_2(\pi_4-\pi_1)\right\}
\end{aligned}$$

$$\begin{aligned}
150(1-R_\rho)^2A_3 &= \pi_1[5\pi_2\pi_4(30\pi_3+17) + \pi_1(15\pi_3+7)]\left(R_\rho^2+1\right)\\
&\quad-(15\pi_3+7)(\pi_1^2-\pi_4^2) - [10\pi_1\pi_3\pi_4(15\pi_3+17)\\
&\quad+15\pi_2(\pi_1^2+\pi_4^2) + 14\pi_1\pi_4(1-10\pi_2)]R_\rho
\end{aligned}$$

$$\begin{aligned}
9000(1-R_\rho)A_4 &= [150(\pi_1\pi_3+\pi_2\pi_4) - 7\pi_1(1+30\pi_1)]R_\rho\\
&\quad-150(\pi_1\pi_2+\pi_3\pi_4) + 7\pi_4(1+30\pi_4)
\end{aligned}$$

$$\begin{aligned}
30(1-R_\rho)A_5 &= [-30(\pi_1\pi_3+\pi_2\pi_4) - 17\pi_1]R_\rho\\
&\quad+30(\pi_1\pi_2+\pi_3\pi_4) + 17\pi_4,\\
A_6 &= -1/60
\end{aligned} \tag{B.12}$$

The π's are given by Eq. (A.11).

Dissipation

Mixed layer:

$$\varepsilon = B_1^2(\tau\Sigma)^{-3}\ell^2\Sigma^3, \quad \ell = \ell_B\left(1-\frac{R_f}{R_{f\infty}}\right)^{4/3},$$

$$\ell_B = \kappa z\ell_0(\ell_0+\kappa z)^{-1} \tag{B.13—B.15}$$

where $\ell_0 = 0.17H$, $\kappa = 0.4$ is the von Karman constant and H is the ML depth computed as the point where the potential density and the surface value differ by $|\sigma(H) - \sigma(0)| > 3\times10^{-5}$ g cm^{-3}; R_f is defined in Eq. (42) and $B_1 = 21.6$.

Thermocline:

$$\varepsilon = \varepsilon_{\text{igw}}L(\theta,N) \tag{B.16}$$

the dimensionless function $L(\theta,N)$ is given by Eq. (65b), the expression for $\varepsilon_{\text{igw}}N^{-2}$ is taken from the Gregg–Henyey–Polzin model, Eq. (66).

Tides

$$\rho\varepsilon_{\text{tides}} = qE(x,y)F(z), \qquad E(x,y) = \frac{1}{2}\bar{\rho}N\kappa h^2\overline{\mathbf{u}_t^2} \tag{B.17}$$

where the wavenumber $\kappa = 2\pi/10$ km and h is the roughness scale obtained from Smith and Sandwell (1997). The scale function $F(z)$ has an exponential shape with a spatial decay scale of $\zeta = 500$ m:

$$F(z) = A\zeta^{-1}\exp[-(H+z)/\zeta], \quad A^{-1} \equiv 1 - \exp[-H/\zeta] \tag{B.18}$$

Bottom drag

$$\boldsymbol{\tau}_b = C_D\bar{\mathbf{u}}\left(\bar{\mathbf{u}}^2 + \overline{\mathbf{u}_t^2}\right)^{1/2}, \quad C_D = 0.003 \tag{B.19}$$

Unresolved bottom shear

In the BBL, the Ri that appears in Eq. (B.1) must be taken to be:

$$\begin{aligned}
&Ri = \frac{N^2}{\Sigma^2}, \quad \Sigma^2 = \Sigma_{\text{res}}^2 + \Sigma_{\text{unr}}^2, \quad \Sigma_{\text{unr}} = \frac{u_*}{\kappa z}\Phi_m,\\
&u_*^2 = C_D\left(\overline{\mathbf{u}_t^2}\right)^{1/2}\left(\bar{\mathbf{u}}^2 + \overline{\mathbf{u}_t^2}\right)^{1/2}
\end{aligned} \tag{B.20}$$

where the function Φ_m is given by Eq. (36) of Cheng et al. (2002).

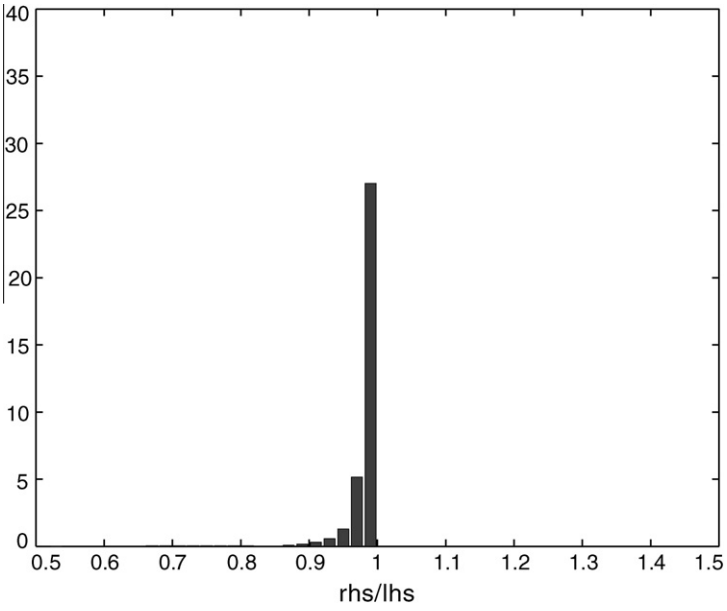

Fig. 11a. Area weighted histogram of the ratio of the rhs to the lhs of the relation for the mean magnitude of the unresolved stress, Eq. (C.8). For details, see text.

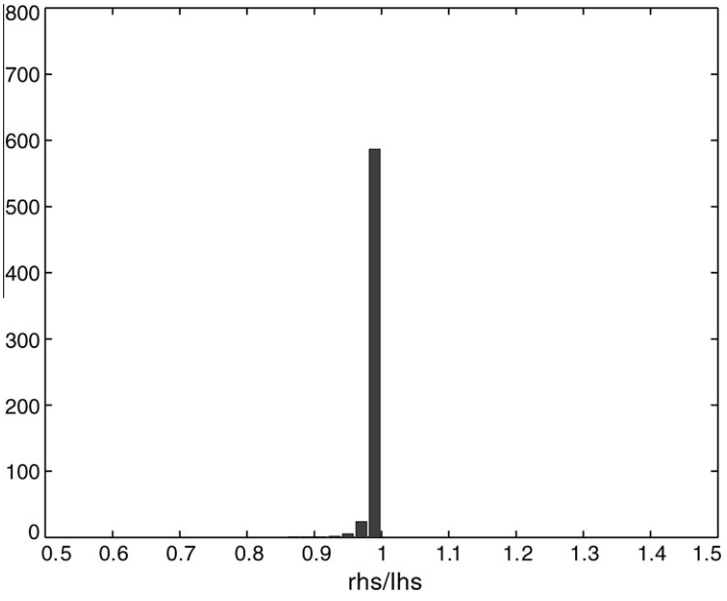

Fig. 11b. Same as in Fig. 11a but the histogram is weighted by the product of the area and the lhs of Eq. (C.8).

Appendix C. Relations (72) and (76)

The total velocity field is contributed by mean and tidal velocities:

$$\boldsymbol{\tau}_b(\text{total}) = C_D \mathbf{u}|\mathbf{u}|, \quad \mathbf{u} = \bar{\mathbf{u}} + \mathbf{u}_t \tag{C.1}$$

We use an overbar to denote the averages used in OGCMs, $\bar{\mathbf{u}}_t = 0$ and $\overline{\mathbf{u}_t|\bar{\mathbf{u}} + \mathbf{u}_t|} = 0$ since by symmetry the latter vector can only point along the direction of $\bar{\mathbf{u}}$ and, to the extent that the mean and tidal fields are uncorrelated (because they represent low and high frequency fields), we expect such a term to vanish. We then obtain:

$$\overline{\boldsymbol{\tau}_b(\text{total})} = C_D \bar{\mathbf{u}} \overline{\left(\bar{\mathbf{u}}^2 + 2\bar{\mathbf{u}} \cdot \mathbf{u}_t + \mathbf{u}_t^2\right)^{1/2}} \tag{C.2}$$

Next, we neglect the second term in the parenthesis since it is the product of high and low frequency variables with little overlap thus giving a zero mean. Eq. (C.2) then becomes:

$$\overline{\boldsymbol{\tau}_b(\text{total})} = C_D \bar{\mathbf{u}} \overline{\left(\bar{\mathbf{u}}^2 + \mathbf{u}_t^2\right)^{1/2}} \tag{C.3}$$

If one exchanges the square root with the averaging process, one obtains Eq. (72). Numerical experiments by Saunders (1977) suggest that even in the worst case the error in making this approximation is no more than 50%. By contrast ignoring the tidal contribution to the drag altogether, as done in most OGCMs to date, can lead to an error of an order of magnitude. As for Eq. (76), we begin with Eq. (C.1). Writing $\bar{\mathbf{u}}^2$ for $\bar{\mathbf{u}} \cdot \bar{\mathbf{u}}$, we have:

$$\boldsymbol{\tau}_\mathbf{b}(\text{total}) = C_D(\bar{\mathbf{u}} + \mathbf{u}_\mathbf{t})\left(\bar{\mathbf{u}}^2 + 2\bar{\mathbf{u}} \cdot \mathbf{u}_\mathbf{t} + \mathbf{u}_t^2\right)^{1/2} \tag{C.4}$$

In order to exhibit the contribution of the unresolved scales, we subtract from (C.4) its average yielding the unresolved part:

$$\boldsymbol{\tau}_b(\mathrm{unr}) = \boldsymbol{\tau}_b(\mathrm{total}) - \overline{\boldsymbol{\tau}_b(\mathrm{total})} \tag{C.5}$$

from which we derive u^* as follows:

$$u_*^2 \equiv \overline{\left[\boldsymbol{\tau}_b^2(\mathrm{unr})\right]^{1/2}} \tag{C.6}$$

Thus, the procedure consists of taking the modulus of (C.5) and averaging it over the OGCM scale. Even adopting the approximations used in (C.3), the expression for $\boldsymbol{\tau}_b^2(\mathrm{unr})$ turns out to be still rather complex:

$$C_D^{-2}\boldsymbol{\tau}_b^2(\mathrm{unr}) = \left(\bar{\mathbf{u}}^2 + \mathbf{u}_t^2\right)^2 + \bar{\mathbf{u}}^2 \Delta^2 - 2\bar{\mathbf{u}}^2\left(\bar{\mathbf{u}}^2 + \mathbf{u}_t^2\right)^{1/2}\Delta,$$
$$\Delta \equiv \overline{\left(\bar{\mathbf{u}}^2 + \mathbf{u}_t^2\right)^{1/2}} \tag{C.7}$$

A similar approximation to the one that led from (C.2) to (70), yields:

$$u_*^2 = \left[\overline{\boldsymbol{\tau}_b^2(\mathrm{unr})}\right]^{1/2} = C_D\left(\overline{\mathbf{u}_t^4} + \bar{\mathbf{u}}^2\overline{\mathbf{u}_t^2}\right)^{1/2}$$
$$\Rightarrow C_D\overline{\mathbf{u}_t^2}^{1/2}\left(\overline{\mathbf{u}_t^2} + \bar{\mathbf{u}}^2\right)^{1/2} \tag{C.8}$$

where the last approximation was necessary because we lack data on $\overline{\mathbf{u}_t^4}$. The last relation is (76).

Lacking access to fine time and space scales ocean velocities field data including mean and tidal components, we tested the above approximation using simulated data. The latter were created by interpolating the velocities from our $3 \times 3^\circ$ NCAR OGCM similar to that used in Canuto et al. (2004b) to the $1/2 \times 1/2^\circ$ grid of the tidal model and then adding at each tidal gridbox a linearly polarized sinusoidal in time velocity field with rms magnitude equal to that of the time-averaged tidal velocity square of the tidal model's output. Four polarizations, east, northeast, north and northwest were used and 12 time steps were taken. We then computed the left- and right-hand sides of (C.8) from the simulated data for each of the polarizations, where the overbar was taken to be an average over time and the $3 \times 3^\circ$ gridcell. The rhs of (C.4) was substituted into (C.5) to compute $\boldsymbol{\tau}_b(\mathrm{unr})$ which was then substituted into the lhs of (C.7). Finally, the ratio of the rhs to the lhs of (C.8) was computed for each polarization for each gridbox. The average weighted either by gridbox area or gridbox area times the lhs of (C.8) was 0.99. Histograms of this ratio with the former and latter weighting are presented in Fig. 11, respectively. We consider the results adequate empirical evidence of the validity of (76) in the context in which we are applying it.

References

Arbic, B.K., Garner, S.T., Hallberg, R.W., Simmons, H.L., 2004. The accuracy of surface elevation in forward global barotropic and barcoclinic tide models. Deep Sea Res. II 51, 3069–3101.

Beckmann, A., 1998. The representation of bottom boundary layer processes in numerical ocean circulation models. In: Chassignet, E.P., Verron, J. (Eds.), Ocean Modelling and Parameterization. Kluwer, Dordrecht, pp. 135–154.

Bertin, F., Barat, J., Wilson, R., 1997. Energy dissipation rates, eddy diffusivity, and the Prandtl number: an in situ experimental approach and its consequences on radar estimate of turbulent parameters. Radio Sci. 32, 791–804.

Blackadar, A.K., 1962. The vertical distribution of wind and turbulent exchange in neutral atmosphere. J. Geophys. Res. 67, 3095–3102.

Burchard, H., 2002. Applied turbulence modeling in marine waters. Lectures Notes in Earth Sciences, vol. 100. Springer, Berlin.

Businger, J.A., Wyngaard, J.C., Izumi, Y., Bradley, E.F., 1971. Flux profile relationship in the atmospheric boundary layer. J. Atmos. Sci. 28, 181–189.

Canuto, V.M., 1992. Turbulent convection with overshooting: Reynolds stress approach. Astrophys. J. 392, 218–232.

Canuto, V.M., 1997. Compressible turbulence. Astrophys. J. 482, 827–851.

Canuto, V.M., Dubovikov, M.S., 1996. A dynamical model for turbulence: I. General formalism. Phys. Fluids 8 (2), 571–586.

Canuto, V.M., Howard, A., Cheng, Y., Dubovikov, M.S., 2001. Ocean turbulence. Part I: one point closure model, momentum and heat vertical diffusivities. J. Phys. Oceanogr. 31, 1413–1426. cited as model I.

Canuto, V.M., Howard, A., Cheng, Y., Dubovikov, M.S., 2002. Ocean turbulence. Part II: vertical diffusivities of momentum, heat, salt, mass and passive scalars. J. Phys. Oceanogr. 32, 240–264. cited as model II.

Canuto, V.M., Howard, A., Hogan, P., Cheng, Y., Dubovikov, M.S., Montenegro, L.M., 2004a. Modeling ocean deep convection. Ocean Modell. 7, 75–95.

Canuto, V.M., Howard, A., Cheng, Y., Miller, R.L., 2004b. Latitude-dependent vertical mixing and the tropical thermocline in a global OGCM. Geophys. Res. Lett. 31, L16305. doi:10.1029/2004GL019891.

Canuto, V.M., Cheng, Y., Howard, A.M., 2005. What causes the divergences in local second-order closure models? J. Atmos. Sci. 62, 1645–1651.

Canuto, V.M., Cheng, Y., Howard, A.M., Esau, I.N., 2008a. Stably stratified flows: a model with no Ri(cr). J. Atmos. Sci. 65, 2437–2447.

Canuto, V.M., Cheng, Y., Howard, A.M., 2008b. A new model for double diffusion + turbulence. Geophys. Res. Lett. 35, L02613. doi:10.1029/2007GL032580.

Canuto, V.M., Cheng, Y., Howard, A.M., 2010. An attempt to derive the ε equation from a two-point closure, J. Atmos. Sci. 67, 1678–1685.

Cheng, Y., Canuto, V.M., Howard, A.M., 2002. An improved model for the turbulent PBL. J. Atmos. Sci. 59, 1550–1565.

Cheng, Y., Canuto, V.M., Howard, A.M., 2005. Non-local convective PBL model based on new third- and fourth-order moments. J. Atmos. Sci. 62, 2189–2204.

Chou, P.Y., 1945. On velocity correlations and the solutions of the equations of turbulent fluctuation. Quart. J. Appl. Math. 3, 38–54.

Craig, P.D., Banner, M.L., 1994. Modelling wave-enhanced turbulence in the ocean surface layer. J. Phys. Oceanogr. 24, 2546–2559.

Deardorff, J.W., 1966. The counter-gradient heat flux in the lower atmosphere and in the laboratory. J. Atmos. Sci. 23, 503–505.

Decloedt, T., Luther, D.S., 2010. On a simple empirical parameterization of topography-catalyzed diapycnal mixing in the abyssal ocean. J. Phys. Oceanogr. 40, 487–508.

Donaldson, duP., 1973. Construction of a dynamic model of the production of atmospheric turbulence and the dispersal of atmospheric pollutants. In: Hauge, D.A. (Ed.), Workshop of Micrometeorology, American Meteorological Society, Boston, MA, pp. 313–392.

Döös, K., Coward, A., 1997. The Southern Ocean as the major upwelling of North Atlantic Deep water. Int. WOCE Newletters 27, 3–4.

Döös, K., Webb, D.J., 1994. The Deacon cell and other meridional cells in the Southern Ocean. J. Phys. Oceanogr. 24, 429–442.

Eden, A., Greatbatch, R.J., 2008a. Diapycnal mixing by mesoscale eddies. Ocean Modell. 23, 113–120.

Eden, C., Greatbatch, R.J., 2008b. Diapycnal mixing by mesoscales. Ocean Modell. 23, 113–120.

Egbert, G.D., Ray, R.D., 2000. Significant dissipation of tidal energy in the deep ocean inferred from satellite data. Nature 405, 775–778.

Egbert, D.G., Ray, R.D., 2003. Semi-diurnal and diurnal tidal dissipation from TOPEX/Poseidon altimetry. Geophys. Res. Lett. 30. doi:10.1029/2003GL017676.

Egbert, G.D., Bennett, A.F., Foreman, M.G.G., 1994. TOPEX/POSEIDON tides estimated using a global inverse model. J. Geophys. Res. 99 (C12), 24821–24852.

Egbert, G.D., Ray, R.D., Bills, B.G., 2004. Numerical modeling of the global semidiurnal tide in the present day and in the last glacial maximum. J. Geophys. Res. 109, C03003. doi:10.1029/2003JC001973.

Frisch, U., 1995. Turbulence: The Legacy of A.N. Kolmogorov. Cambridge University Press, New York. Section 5.2, 296pp.

Garrett, C., Kunze, E., 2007. Internal tide generation in the deep ocean. Annu. Rev. Fluid Mech. 39, 57–87.

Garrett, C., St. Laurent, L., 2002. Aspects of deep ocean mixing. J. Oceanogr. 58, 11–24.

Gerz, T., Schumann, U., Elghobashi, S.E., 1989. Direct numerical simulation of stratified, homogenous turbulent shear flows. J. Fluid Mech. 220, 563–594.

Gregg, M.C., Winkel, D.P., Sanford, T.S., Peters, H., 1996. Turbulence produced by internal waves in the ocean thermocline at mid and low latitudes. Dyn. Atmos. Oceans 24, 1–14.

Gregg, M.C., Sanford, T.B., Winkel, D.P., 2003. Reduced mixing from breaking of internal waves in equatorial waters. Nature 422, 513–515.

Griffies, S.M., Gnanadesikan, A., Dixon, K.W., Dunne, J.P., Gerdes, R., Harrison, M.J., Rosati, A., Russell, J.L., Samuels, B.L., Spelman, M.J., Winton, M., Zhang, R., 2005. Formulation of an ocean model for global climate simulations. Ocean Sci. 1, 45–79.

Haidvogel, D.B., Beckmann, A., 1999. Numerical Ocean Circulation Modeling. Imperial College Press, London. 318pp.

Holtslag, A.A.M., Moeng, C.-H., 1991. Eddy diffusivity and counter-gradient transport in the convective atmospheric boundary layer. J. Atmos. Sci. 48, 1690–1700.

Inoue, R., Yamakazi, H., Wolk, F., Kono, T., Yoshida, J., 2007. An estimation of buoyancy flux for a mixture of turbulence and double diffusion. J. Phys. Oceanogr. 37, 611–624.

Jayne, S.R., 2009. The impact of abyssal mixing parameterizations in an ocean general circulation model. J. Phys. Oceanogr. 39, 1756–1775.

Jayne, S.R., St. Laurent, L.C., 2001. Parameterizing tidal dissipation over rough topography. Geophys. Res. Lett. 28, 811–814.

Kaimal, J.C., Finnigan, J.J., 1994. Atmospheric Boundary Layer Flows. Oxford University Press, New York. 289pp.

Kantha, L.H., Tierney, C.G., 1997. Global baroclinic tides. Prog. Oceanogr. 40, 163–178.

Kantha, L.H., Desai, S.D., Lopez, J.W., Tierney, C., Parke, M., Drexler, L., 1995. Barotropic tides in the global oceans from a non-linear model assimilating

altimetric tides. Part 2: altimetric and geophysical implications. J. Geophys. Res. 100, 25309–25317.
Kelley, D.E., 1990. Fluxes through diffusive staircases: a new formulation. J. Geophys. Res. 95, 3365–3371.
Kelley, D.E., 2001. Six question about double-diffusive convection. In: Muller, P., Garrett, C. (Eds.), From stirring to Mixing in a Stratified Ocean: 12th Aha Huliko', Hawaiian Winter Workshop, University of Hawaii.
Kelley, D.E., Fernando, H.J.S., Gargett, A.E., Tanny, J., Ozsoy, E., 2003. The diffusive regime of double-diffusion convection. Oceanography 56, 461–481.
Klocker, A., McDougall, T.J., 2010. The influence of the nonlinear equation of state on global estimates of dianeutral advection and diffusion. J. Phys. Oceanogr., in press.
Kolmogorov, A.N., 1941, The local structure of turbulence in incompressible viscous fluid for very large Reynolds number, Dokl. Akad. Nauk SSSR, 30, 9–13. Reprinted in Proc. R. Soc. Lond. Ser., A 434, 9–13, 1991.
Kondo, J., Kanechika, O., Yasuda, N., 1978. Heat and momentum transfer under strong stability in the atmospheric surface layer. J. Atmos. Sci. 35, 1012–1021.
Kunze, E., 2003. A review of oceanic salt-fingering theory. Oceanography 56, 399–417.
Kunze, E., Sanford, T.S., 1996. Abyssal mixing: where it is not? J. Phys. Oceanogr. 26, 2286–2296.
Kunze, E., Firing, E., Hummon, J.M., Thurnherr, A.M., 2006. Global abyssal mixing inferred from lowered ADCP shear and CDT strain profiles. J. Phys. Oceanogr. 36, 1553–1576.
Large, W.G., McWilliams, J.C., Doney, S.C., 1994. Oceanic vertical mixing. A review with non-local boundary layer parameterization. Rev. Geophys. 32, 363–403.
Large, W.G., Danabasoglu, G., Doney, S.C., McWilliams, J.C., 1997. Sensitivity to surface forcing and boundary layer mixing in a global ocean model: annual-mean climatology. J. Phys. Oceanogr. 27, 2418–2447.
Ledwell, J.R., Watson, A.J., Law, C.S., 1993. Evidence for slow mixing across the pycnocline from open ocean tracer release experiment. Nature 364, 701–703.
Ledwell, J.R., Wilson, A.J., Law, C.S., 1998. Mixing of a tracer released in the pycnocline of a subtropical gyre. J. Geophys. Res. 103, 21499–21529.
Lee, H.-C., Rosati, A., Spelman, M., 2006. Barotropic tidal mixing effects in a coupled climate model: oceanic conditions in the Northern Atlantic. Ocean Modell. 11, 464–477.
Legg, S., 2004. Internal tides generated on a corrugated continental slope. Part I: cross-slope barotropic forcing. J. Phys. Oceanogr. 34, 156–173.
Linden, P.F., 1971. Salt fingers in the presence of grid-generated turbulence. J. Fluid Mech. 49, 611–624.
Llewellyn Smith, S.G., Young, W.R., 2002. Conversion of the barotropic tide. J. Phys. Oceanogr. 32, 1554–1566.
Mahadevan, A., Tandon, A., Ferrari, R., 2010. Rapid changes in mixed layer stratification driven by submesoscale instabilities and winds. J. Geophys. Res. 115, CO3017, 12, pp. doi:10.1029/2008JC005203.
Martin, P., 1985. Simulation of the mixed layer at OWS November and Papa with several models. J. Geophys. Res. 90, 903–916.
Mellor, G.L., Yamada, T., 1982. Development of a turbulence closure model for geophysical fluid problems. Rev. Geophys. Space Phys. 20, 851–875.
Moeng, C.-H., Sullivan, P.P., 1994. A comparison of shear and buoyancy drive planetary boundary layer flows. J. Atmos. Sci. 51, 999–1022.
Monin, A.S., Yaglom, A.M., 1971. Statistical Fluid Dynamics, vol. 1. MIT Press, Cambridge, MA. 769pp.
Muench, R.D., Fernando, H.J.S., Stegen, G.R., 1990. Temperature and salinity staircases in the Northern Weddell Sea. J. Phys. Oceanogr. 20, 295–306.
Munk, W.H., 1966. Abyssal recipes. Deep Sea Res. 13, 707–730.
Munk, W.H., 1997. Once again: once again-tidal friction. Prog. Oceanogr. 40, 7–35.
Munk, W.H., Bills, B., 2007. Tides and climate: some speculations. J. Phys. Oceanogr. 37, 135–147.
Munk, W.H., Wunsch, C., 1998. Abyssal recipes II: energetics of tidal and wind mixing. Deep Sea Res. I 45, 1977–2110.
Oakey, N.S., 1985. Statistics of mixing parameters in the upper ocean during JASIN phase 2. J. Phys. Oceanogr. 15, 1662–1675.
Ohya, Y., 2001. Wind-tunnel study of atmospheric stable boundary layers over a rough surface. Boundary-Layer Meteorol. 98, 57–82.
Osborn, T.R., 1980. Estimates of the local rate of vertical diffusion from dissipation measurements. J. Phys. Oceanogr. 10, 83–89.
Oschlies, A., 2002. Improved representation of upper-ocean dynamics and mixed layer depths in a model of the North Atlantic on switching from eddy-permitting to eddy resolving grid resolution. J. Phys. Oceanogr. 32, 2277–2298.
Pacanowski, R., Philander, S.G.H., 1981. Parameterization of vertical mixing in numerical models of tropical oceans. J. Phys. Oceanogr. 11, 1443–1451.
Polzin, K., 1996. Statistics of the Richardson number, mixing models and fine structure. J. Phys. Oceanogr. 26, 1409–1425.
Polzin, K., Toole, J.M., Schmitt, R.W., 1995. Finescale parameterization of turbulent dissipation. J. Phys. Oceanogr. 25, 306–328.
Pope, S.B., 2000. Turbulent Flows. Cambridge University Press, New York, NY. 771pp.
Rehman, C.R., Koseff, J.R., 2004. Mean potential energy change in stratified grid turbulence. Dyn. Atmos. Oceans 37, 271–294.
Reynolds, O., 1895. On the dynamical theory of incompressible viscous fluids and the determination of the criterion. Phil. Trans. R. Soc. Lond. Ser., A 1186, 123–164.
Richardson, L.F., 1926, Atmospheric diffusion shown on a distance-neighbour graph. Proc. Roy. Soc. Ser., A 110, 709–737. Also available in Collected Papers of L.F. Richardson. In: Drazin, P.G. (Ed.), vol. 1, Cambridge University Press, Cambridge, pp. 523–551.
Ruddick, B., Gargett, A.E., 2003. Oceanic double-diffusion: introduction. Progr. Oceanogr. 56, 381–393.
Saenko, O.A., Merryfield, W.J., 2005. On the effect of topographically enhanced mixing on the global ocean circulation. J. Phys. Oceanogr. 35, 826–834.
Saunders, P.M., 1977. Average drag in an oscillatory flow. Deep Sea Res. 24, 381–384.
Schmitt, R.W., 1994. Double diffusion in oceanography. Annu. Rev. Fluid Mech. 26, 255–285.
Schmitt, R.W., 2003. Observational and laboratory insights into salt fingers convection. Progr. Oceanogr. 56, 419–433.
Schmitt, R.W., Evans, D.L., 1978. An estimate of the vertical mixing due to salt fingers based on observations in the North Atlantic Central Water. J. Geophys. Res. 83, 2913–2919.
Schumann, U., Gerz, T., 1995. Turbulent mixing in stably stratified shear flows. J. Appl. Meteorol. 34, 33–48.
Simmons, H.L., Jayne, S.R., St. Laurent, L.C., Weaver, A.J., 2004. Tidally driven mixing in a numerical model of the ocean general circulation. Ocean Modell. 6, 245–263.
Smith, W.H.F., Sandwell, D.T., 1997. Global sea floor topography from satellite altimetry and ship data soundings. Science 277, 1956–1962.
Smyth, W.D., Kimura, S., 2007. Instability and diapycnal momentum transfer in double diffusive, stratified shear layer. J. Phys. Oceanogr. 37, 1551–1565.
St. Laurent, L., Garrett, C., 2002. The role of internal tides in mixing the deep ocean. J. Phys. Oceanogr. 32, 2882–2899.
St. Laurent, L., Schmitt, R.W., 1999. The contribution of salt fingers to vertical mixing in the North Atlantic tracer release experiment. J. Phys. Oceanogr. 29, 1404–1424.
St. Laurent, L., Simmons, H.L., Jayne, S.R., 2002. Estimating tidally driven mixing in the deep ocean. Geophys. Res. Lett. 29 (23), 2106. doi:10.1029/2002GL015633.
Strang, E.J., Fernando, H.J.S., 2001. Vertical mixing and transports through a stratified shear layer. J. Phys. Oceanogr. 31, 2026–2048.
Stretch, D.D., Rottman, J.W., Nomura, K.K., Venayagamoorthy, S.K., 2001. Transient mixing events in stably stratified turbulence, In: 14th Australasian Fluid Mechanics Conference, Adelaide, Australia, 10–14 December 2001.
Tandon, A., Garrett, C., 1996. On a recent parameterization of mesoscale eddies. J. Phys. Oceanogr. 26, 406–411.
Toggweiler, J.R., Samuels, B., 1998. On the ocean's large-scale circulation near the limit of no vertical mixing. J. Phys. Oceanogr. 28, 1832–1852.
Toole, J.M., 1998. Turbulent mixing in the ocean. In: Chassignet, E.P., Verron, J. (Eds.), Ocean Modeling and Parameterization. NATO, ASI, Series C, vol. 516. Kluwer Academic Publishers, Hingham, MA, pp. 171–190.
Umlauf, L., Burchard, H., 2005. Second-order turbulence closure models for geophysical boundary layers. A review of recent work. Continen. Shelf Res. 25, 795–827.
Walsh, D., Ruddick, B., 2000. Double-diffusion interleaving in the presence of turbulence: the effect of a non-constant flux ratio. J. Phys. Oceanogr. 30, 2231–2245.
Webb, D.J., Suginohara, N., 2001a. The interior circulation of the ocean. In: Siedler, G., Church, J., Gould, J. (Eds.), Ocean Circulation and Climate. Academic Press, New York.
Webb, D.J., Suginohara, N., 2001b. Oceanography: vertical mixing in the ocean. Nature 409, 37–38.
Webster, C.A.G., 1964. An experimental study of turbulence in a stratified shear flow. J. Fluid Mech. 19, 221–245.
Zang, X., Wunch, C., 2001. Spectral description of low frequency oceanic variability. J. Phys. Oceanogr. 31, 3073–3095.
Zeman, O., Lumley, J.L., 1982. Modeling salt-fingers structures. J. Mar. Res. 40, 315–330.
Zhang, J., Huang, R.X., 1998. Sensitivity of the GFDL ocean model to parameterization of double-diffusion processes. J. Phys. Oceanogr. 28, 589–605.
Zilitinkevich, S.S., Elperin, T., Kleeorin, N., Rogachevskii, I., 2007. Energy- and flux-budget (EFB) turbulence closure model for the stably stratified flows. Part I: steady-state, homogeneous regimes. Boundary-Layer Meteorol. 125, 167–192. doi:10.1007/s10546-007-9189-2.
Zilitinkevich, S.S., Elperin, T., Kleeorin, N., Rogachevskii, I., Esau, I., Mauritsen, T., et al., 2008. Turbulence energetics in stably stratified geophysical flows: Strong and weak mixing regimes. Quarterly J. Royal Meteorol. Soc. 134, 793–799. d.o.i: 101002/qj.264.